kinases and phosphatases

MDPI

Article

MAP3K4 Kinase Activity Is Important for Placental Trophoblast Responses During Cell Differentiation

Nathan A. Mullins, Patrick A. Roberto, Amya T. Sallee and Amy N. Abell *

Department of Biological Sciences, University of Memphis, Memphis, TN 38152, USA; nmllins1@memphis.edu (N.A.M.); proberto@memphis.edu (P.A.R.); atsallee@memphis.edu (A.T.S.)
* Correspondence: anabell@memphis.edu

Abstract

During development, stem cells rapidly proliferate and differentiate to form the embryo and the placenta, requiring intensive increases in cellular protein synthesis and changes to the cell architecture. Chaperone proteins, including the small heat shock proteins (HSPs), are critical assistants to protein folding, preventing protein aggregation, and promoting autophagy. Mitogen-activated protein kinase kinase kinase 4 (MAP3K4) is a stress-activated kinase that promotes fetal and placental growth. MAP3K4 directly activates p38 and JNK in trophoblast stem (TS) cells by phosphorylating MAP2K3 and MAP2K4/7, respectively. In addition, MAP3K4 promotes activation of the Akt signaling pathway by controlling *Igf1r* expression. TS cells differentiate to placental trophoblasts comprising the junctional zone (JZ) and labyrinth (LAB) placental layers. In this study, we demonstrate that JZ differentiation transiently increases JNK activity, whereas LAB differentiation induces sustained p38, JNK, and Akt activation. Each of these pathways is inhibited in MAP3K4 kinase-inactive (KI) LAB^{KI} trophoblasts. JZ and LAB differentiation also induces HSP22 and HSP27 expression and HSP27 phosphorylation; these are also reduced in TS^{KI} and LAB^{KI} cells. JZ and LAB differentiation induces GABARAP-positive autophagosomes that are deficient in KI cells. Altogether, our findings demonstrate that MAP3K4 is critical for responses during differentiation in placental trophoblasts.

Keywords: differentiation; FGR; HSP22; HSP27; MAP3K4; MAPK; placenta; stem cells; autophagy; trophoblasts

1. Introduction

The placenta is an organ that serves as an interface between the mother and fetus, allowing for active transport of nutrients and hormones necessary for proper fetal development. Placental insufficiency, which arises from disrupted placental function, can lead to fetal growth restriction (FGR) [1–4]. As an extraembryonic organ, the placenta is primarily composed of trophoblasts formed by differentiation of trophoblast stem (TS) cells derived from the trophectoderm of the blastocyst. Fetal endothelial cells and maternal decidual cells are also present in the placenta [1,2]. TS cells differentiate to form all trophoblasts found within the junctional zone (JZ) and labyrinth (LAB) layers of the placenta. JZ trophoblasts exhibit mesenchymal, invasive characteristics, while LAB trophoblasts facilitate transport of nutrients and gases between the maternal and fetal vasculature [1,2,5,6]. In the presence of stemness-maintaining factors, TS cells can be cultured in vitro for an indefinite period; removal of these factors induces differentiation of TS cells to JZ trophoblasts [5,6]. LAB trophoblasts can be formed by differentiating TS cells in the presence of CHIR99021, a GSK3

Check for updates

Academic Editor: Mauro Salvi

Received: 9 April 2026
Revised: 23 May 2026
Accepted: 28 May 2026
Published: 5 June 2026

Copyright: © 2026 by the authors. Licensee MDPI, Basel, Switzerland. This article is an open access article distributed under the terms and conditions of the Creative Commons Attribution (CC BY) license.

inhibitor [7]. These cells exhibit significantly increased LAB marker expression, including *Cdh1*, *Gcm1,* and *Synb*, and syncytialization when compared to the JZ cells, resulting in a useful in vitro method for studying LAB cells [7,8].

Mitogen-activated protein kinase kinase kinase 4 (MAP3K4) is a member of the MAP3K family of protein kinases and is highly expressed in TS cells [6,9]. MAP3K4 controls important developmental processes, including epithelial-to-mesenchymal transition (EMT) and embryonic and placental growth [6,8,10–12]. Stemness, which is defined as self-renewal and potency, is maintained in TS cells through fibroblast growth factor 4 (FGF4) activation of fibroblast growth factor receptor 1/2 (FGFR1/2) [5,6,13]. Once FGFR1/2 is activated, MAP3K4 directly phosphorylates the mitogen-activated protein kinase kinases (MAP2Ks) MAP2K3/6 and MAP2K4/7, which phosphorylate the mitogen-activated protein kinases (MAPKs) p38 and c-Jun N-terminal kinase (JNK), respectively [9,14–16]. In TS cells, MAP3K4 promotes histone acetylation and gene expression by enhancing CREB-binding protein (CBP) and p300 acetyltransferase activity through p38- and JNK-mediated phosphorylation [10,11,17]. Further, MAP3K4 binds histone deacetylase 6 (HDAC6) and inhibits it by promoting HDAC6 ubiquitination and destruction; one consequence is increased histone acetylation and expression of select genes [8,11,17,18].

To determine the roles of MAP3K4 kinase activity, the active site lysine at position 1361 was mutated to arginine, rendering the protein kinase-inactive (KI) [9]. MAP3K4 KI in TS (TS^{KI}) cells results in ablated MAP3K4 kinase activity and inhibited downstream signaling [6,8,9,19]. Further, TS^{KI} cells exhibit morphological properties of EMT, including increased motility and invasiveness, due in part to increased expression and activity of HDAC6 [6,10–12,17,18,20,21]. The phenotype of mice homozygous for MAP3K4 KI ($Map3k4^{KI/KI}$) is characterized by highly penetrant lethality before weaning as well as exencephaly and spina bifida [8,9]. $Map3k4^{KI/KI}$ embryos and rare surviving mice display male-to-female gonadal sex reversal, caused by suppressed *Sry* and *Sox9* expression, two genes promoted by p38 activity [16]. Recently, our lab discovered $Map3k4^{KI/KI}$ mice exhibit FGR, stemming from placental insufficiency caused in part by reduced expression of the insulin-like growth factor 1 receptor/insulin receptor (IGF1R/IR) and activation of Akt in the placenta [8]. The IGF1R was reduced at both the transcript and protein level in TS^{KI} cells, due to reduced promoter acetylation by CBP and increased promoter deacetylation by HDAC6 [8]. Reduced *Igf1r* expression was responsible in part for reduced Akt activity in TS^{KI} cells [8]. MAP3K4 KI in mice also causes trophoblast hyperinvasion, resulting in defective implantation and reduced placental size and weight [8–10]. The dysregulation of placental function and morphology in $Map3k4^{KI/KI}$ mice demonstrates the importance of MAP3K4 for normal fetal and placental development.

Throughout gestation, the mother, fetus, and placenta all experience stresses that can arise from endogenous and environmental sources [22–24]. In addition to hyperosmotic and hypoxic stresses, proteotoxic stresses can occur due to robust increases in protein synthesis required for generating specialized trophoblast cell types during cellular differentiation [22–24]. Cellular stress plays a key role during normal trophoblast differentiation and placental development, but excessive stress or failure to mediate stress may increase the risk of developmental pathologies such as embryonic lethality and FGR [22–24]. Activation of p38 through MAP3K4 leads to increased levels of phosphorylated heat shock protein 27 (pHSP27) in TS cells [19]. HSP27 is a chaperone protein that helps maintain the folded state of its client proteins in response to stress conditions by acting as holdases to prevent substrate aggregation and by assisting other chaperones in protein refolding [25,26]. In addition, HSP27 can promote the removal and degradation of damaged organelles and misfolded/aggregated proteins through autophagy [27]. HSP27 is also known to regulate important cellular processes such as apoptosis and cytoskeletal remodeling [9,25,28]. The

function of HSP27 within the cell depends on its quaternary structure, where the protein exists as a large oligomer in its unphosphorylated state; phosphorylation of HSP27 promotes the small oligomer structure of the protein and regulates cytoskeletal dynamics and apoptosis under stress conditions [25,28]. In general, the phosphorylated form of HSP27 has the highest chaperone efficiency [29]. Expression of heat shock proteins has been shown to be modulated by stress consistent with potential roles for them in fetal and placental development.

Our lab has previously shown the stress-activated kinase MAP3K4 controls basal p38, JNK, and Akt activity in TS cells, but the role of MAP3K4 in regulation of these pathways in differentiated JZ and LAB trophoblasts is unknown [6,8,19]. Herein, we demonstrate that JNK activation was transiently elevated in JZ trophoblasts, while p38, JNK, and Akt exhibited a sustained increase in activity in LAB trophoblasts. Our data show JNK and p38 activity were decreased in MAP3K4 KI JZ (JZ^{KI}) and MAP3K4 KI LAB (LAB^{KI}) trophoblasts. We discovered that two heat shock proteins, heat shock protein 22 (HSP22) and HSP27, were induced by JZ and LAB trophoblast differentiation. Both JZ^{KI} and LAB^{KI} trophoblasts exhibited reduced HSP22 expression, while LAB^{KI} trophoblasts also showed reduced HSP27 expression. Reduced expression of *Hspb1* and *Hspb8* in KI cells may be due to reduced REL expression in KI cells and may be responsible in part for reduced autophagy in the KI cells. In summary, our data show MAP3K4 is important for responding to stress during cell differentiation to form placental trophoblasts through promotion of p38 and JNK activity as well as HSP22 and HSP27 expression. These findings may help improve therapeutic strategies to treat developmental diseases involving dysregulated responses to stress, including FGR.

2. Results

2.1. Basal TS Cell Activation of p38 and JNK Is Diminished in the Absence of MAP3K4 Kinase Activity

TS cells originate from the trophectoderm of murine E3.5 blastocysts and give rise to all trophoblast cell types that comprise the placenta (Figure S1) [1,2]. In TS cells, p38α (*Mapk14*) and JNK2 (*Mapk9*) are the predominantly expressed p38 and JNK proteins (Table S1). JNK1 and JNK2 are alternatively spliced, resulting in eight potential JNK isoforms with both overlapping and distinct molecular weights [30]. MAP3K4 activates p38 and JNK in TS cells, but it does not directly activate other MAPK proteins such as extracellular signal-regulated kinase (ERK) in these cells [6,8,9,15,19,30,31]. Recently, we discovered the MAP3K4-dependence of the growth- and survival-promoting Akt pathway in TS cells through MAP3K4 activation of CBP acetylation and inhibition of HDAC6 deacetylation of the *Igf1r* promoter [8]. To further examine these pathways in TS cells, we performed Western blotting and densitometry analyses, which supported our previous findings, indicating p38, HSP27, JNK, and Akt phosphorylation were significantly reduced in TS^{KI} cells relative to TS^{WT} cells (Figure 1A–E). Phosphorylation of ERK was not significantly altered in TS^{KI} cells (Figure 1A,F). Of these kinases, p38 was the most significantly inhibited in TS^{KI} cells compared to TS^{WT} cells ($p < 0.0001$), suggesting a role for MAP3K4 kinase activity in basal p38 phosphorylation in TS cells. Stress has also been shown to activate p38 and JNK in TS cells, but the role of MAP3K4 in the response of TS cells to stresses is unknown [32]. Here, we found the addition of sorbitol, an inducer of hyperosmotic stress, to the culture media caused a robust induction of p38 and JNK phosphorylation in TS^{WT} cells, while phosphorylation of Akt increased modestly (Figure 1G). Activation of p38 and JNK by sorbitol was reduced in TS^{KI} cells when compared to TS^{WT} cells, suggesting a role for MAP3K4 in the response to sorbitol in TS cells (Figure 1G). UV exposure resulted in robust increases in p38, JNK, and Akt phosphorylation in TS cells in a MAP3K4-independent

manner (Figure 1H). Taken together, these data suggest a selective role for MAP3K4 kinase activity in the activation of p38 and JNK under basal conditions and hyperosmotic stress.

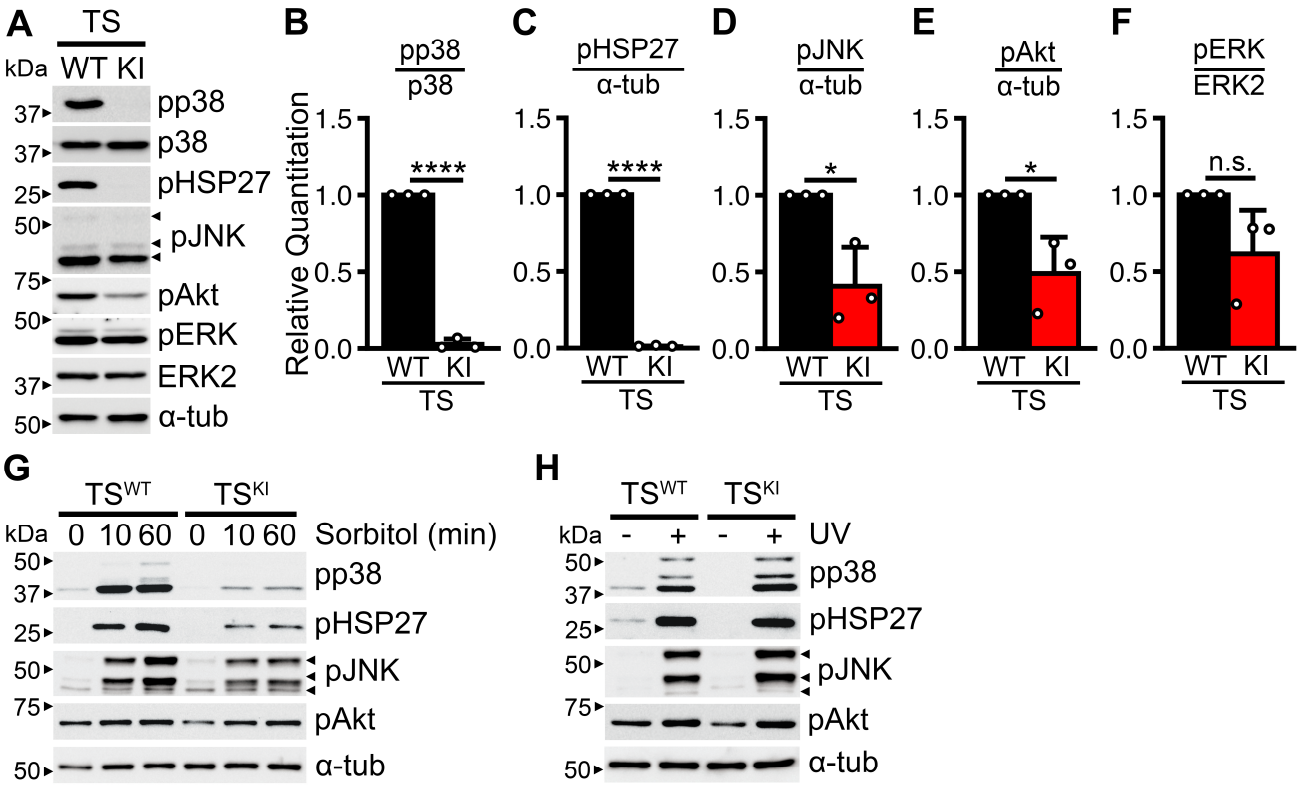


Figure 1. Mitogen-activated protein kinase kinase kinase 4 (MAP3K4) activity is required for activation of stress-related signaling pathways in trophoblast stem (TS) cells. (**A**) MAP3K4 kinase inactivation (KI) in TS (TS^{KI}) cells results in reduced p38, heat shock protein 27 (HSP27), JNK, and Akt phosphorylation relative to WT TS (TS^{WT}) cells. p38, ERK2, and α-tubulin (α-tub) were used as loading controls. (**B**–**F**) Densitometry was used to quantify the mean ± SD of $n = 3$ biologically independent experiments. Normalization was performed as indicated in each plot, where the target proteins are shown as the numerator and the loading controls are displayed as the denominator. Each point indicates one biologically independent experiment. The *p*-value thresholds for Student's *t*-tests are indicated with the following symbols: * [$p < 0.05$], **** [$p < 0.0001$], and not significant (n.s.) [$p > 0.05$]. (**G**) The induction of p38, HSP27, and JNK phosphorylation by sorbitol is MAP3K4-dependent in TS cells, while (**H**) UV activates these pathways in both TS^{WT} and TS^{KI} cells. (**A**,**G**,**H**) Images show representative Western blots from $n = 3$ biologically independent experiments.

2.2. Specific MAP3K4 Pathways Are Induced by Differentiation of TS Cells to the Invasive Placental Cells of the Junctional Zone

Maintenance of stemness in TS cells requires the presence of FGF4, heparin, and mouse embryonic fibroblast-conditioned media (MEF-CM); removal of these components during in vitro culture leads to differentiation of TS cells to JZ trophoblasts (Figure S1). TS cells differentiated by this method preferentially form a heterogeneous population of trophoblast giant cells and spongiotrophoblasts of the JZ, with few syncytiotrophoblasts (SynT) of the LAB present [5,6]. Since trophoblasts experience stress during differentiation due in part to cytoskeletal shape changes and increased protein synthesis, we wondered if MAP3K4-dependent signaling pathways were activated by differentiation of TS cells to JZ trophoblasts. Western blot and densitometry data showed p38 phosphorylation was not significantly induced by JZ differentiation (Figure 2A,B). In contrast, phosphorylation of JNK was weakly and transiently induced with JZ differentiation (Figure 2A,C). Furthermore, Akt phosphorylation was modestly and significantly increased while ERK phosphorylation was significantly decreased, suggesting these kinases are also altered by differentiation of TS

cells to JZ trophoblasts (Figure 2A,D,E). These findings led us to wonder if MAP3K4 impacts these pathways in JZ trophoblasts. Our Western blot and densitometry data showed p38, JNK, and ERK phosphorylation were significantly decreased in 4-day differentiated JZ^{KI} cells when compared to JZ^{WT} cells (Figure 2F–J). Overall, our data indicate JZ trophoblast differentiation induces transient JNK phosphorylation and sustained Akt phosphorylation, and MAP3K4 affects p38, JNK, and ERK signaling in JZ trophoblasts.

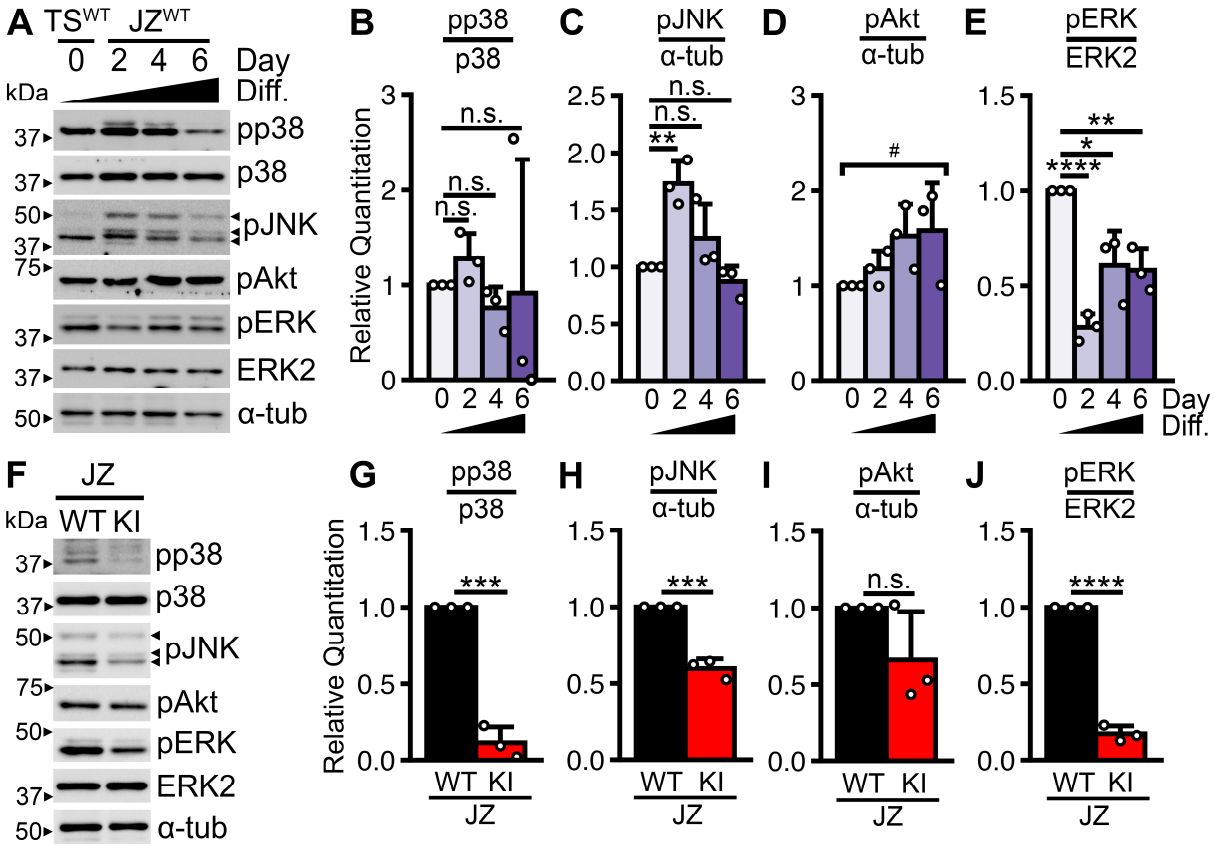


Figure 2. Selective induction of MAP3K4-dependent pathways by differentiation of TS cells to the invasive placental cells of the junctional zone (JZ). (**A**–**E**) Differentiation of TS^{WT} cells to form JZ trophoblasts (JZ^{WT}) altered JNK, Akt, and ERK phosphorylation. (**F**–**J**) MAP3K4 KI in JZ (JZ^{KI}) cells resulted in reduced p38, JNK, and ERK activity relative to JZ^{WT} cells. (**A**,**F**) Representative Western blots and (**B**–**E**,**G**–**J**) densitometry were used to quantify the mean ± SD of $n = 3$ biologically independent experiments. Normalization was performed as indicated in each plot, where the target proteins are shown as the numerator and the loading controls are displayed as the denominator. Each point indicates one biologically independent experiment. (**B**,**C**,**E**,**G**–**J**) The *p*-value thresholds for Student's *t*-tests are indicated with the following symbols: * [$p < 0.05$], ** [$p < 0.01$], *** [$p < 0.001$], **** [$p < 0.0001$], and n.s. [$p > 0.05$]. (**D**) The *p*-value thresholds for one-way ANOVA tests are indicated with the following symbols: # [$p < 0.05$].

2.3. MAP3K4 Kinase Activity Impacts p38, JNK, Akt, and ERK Activity in a Model of the Syncytiotrophoblasts of the Placental Labyrinth

In vivo differentiation of TS cells in mice leads to formation of the SynT cells that comprise the placental LAB [1,2,33,34]. However, removal of stemness factors in vitro is not sufficient to induce SynT formation [5,6]. Removal of the stemness-maintaining factors and addition of CHIR99021, a GSK3 inhibitor, to the culture media robustly induces SynT formation (Figure S1) [7]. Since we found JZ^{WT} differentiation led to modest activation of JNK and Akt, we wondered if MAP3K4-dependent signaling pathways were activated by differentiation of TS^{WT} cells to LAB^{WT} cells. LAB^{WT} trophoblast differentiation resulted in significantly induced, sustained phosphorylation of p38, JNK, and Akt

(Figure 3A–D). In contrast, phosphorylation of ERK significantly decreased in early LAB^{WT} differentiation (Figure 3A,E). Due to our findings showing decreased p38, JNK, and ERK phosphorylation in JZ^{KI} cells relative to JZ^{WT} cells, we wondered if these pathways were MAP3K4-dependent in LAB cells. To examine a role for MAP3K4 on MAPK and Akt signaling in LAB trophoblasts, we compared phosphorylation of these signaling pathways between LAB^{WT} and LAB^{KI} cells. p38, JNK, Akt, and ERK phosphorylation were all significantly decreased in LAB^{KI} cells relative to LAB^{WT} cells, suggesting a role for MAP3K4 in activation of these pathways in the LAB (Figure 3F–J).

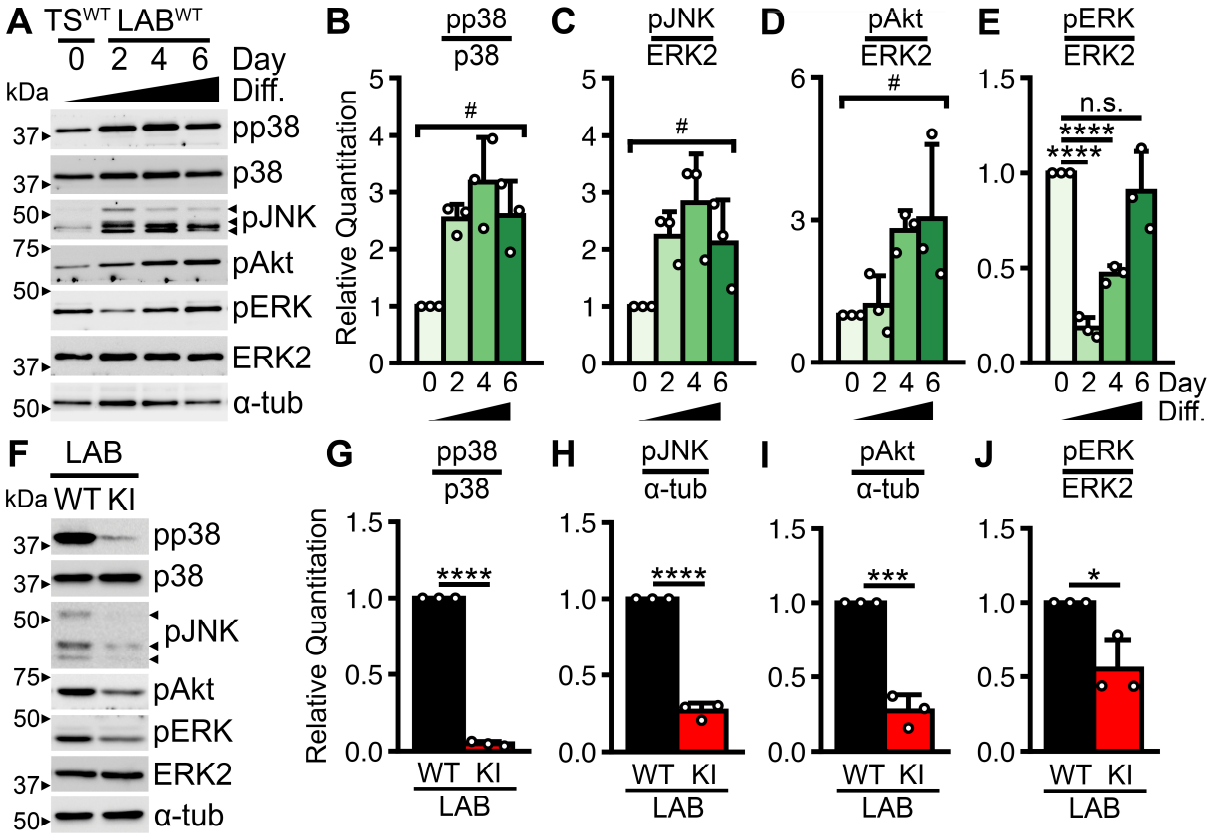


Figure 3. MAP3K4 promotes sustained p38, JNK, and Akt activity in the syncytial cells of the placental labyrinth (LAB). (**A**–**E**) Differentiation of TS^{WT} cells to form LAB trophoblasts (LAB^{WT}) induces p38, JNK, and Akt activity. (**F**–**I**) Phosphorylation of p38, JNK, Akt, and ERK are reduced in KI LAB (LAB^{KI}) trophoblasts when compared to LAB^{WT} trophoblasts. (**A**,**F**) Representative Western blots and (**B**–**E**,**G**–**J**) densitometry were used to quantify the mean ± SD of $n = 3$ biologically independent experiments. Normalization was performed as indicated in each plot, where the target proteins are shown as the numerator and the loading controls are displayed as the denominator. Each point indicates one biologically independent experiment. (**E**,**G**–**J**) The p-value thresholds for Student's t-tests are indicated with the following symbols: * [$p < 0.05$], *** [$p < 0.001$], **** [$p < 0.0001$], and n.s. [$p > 0.05$]. (**B**–**D**) The p-value thresholds for one-way ANOVA tests are indicated with the following symbols: # [$p < 0.05$].

2.4. JNK Activity Is Higher in JZ Trophoblasts, While p38 Activity Is Higher in LAB Trophoblasts

Our data showed weak and transient activation of JNK during JZ^{WT} differentiation and sustained activation of p38, JNK, and Akt during LAB^{WT} differentiation (Figures 2A and 3A). To directly compare these differentiated cell types, we ran 4-day differentiated JZ^{WT} and LAB^{WT} cells side-by-side, finding p38 phosphorylation was significantly higher in LAB^{WT} cells when compared to JZ^{WT} cells (Figure 4A,B). Additionally, JNK phosphorylation was lower in LAB^{WT} cells relative to JZ^{WT} cells (Figure 4A,C). Phosphorylation of Akt and ERK was similar between JZ^{WT} and LAB^{WT} cells (Figure 4A,D–E).

Altogether, our data suggest activation of JNK is higher in JZ trophoblasts and p38 activity is higher in LAB trophoblasts.

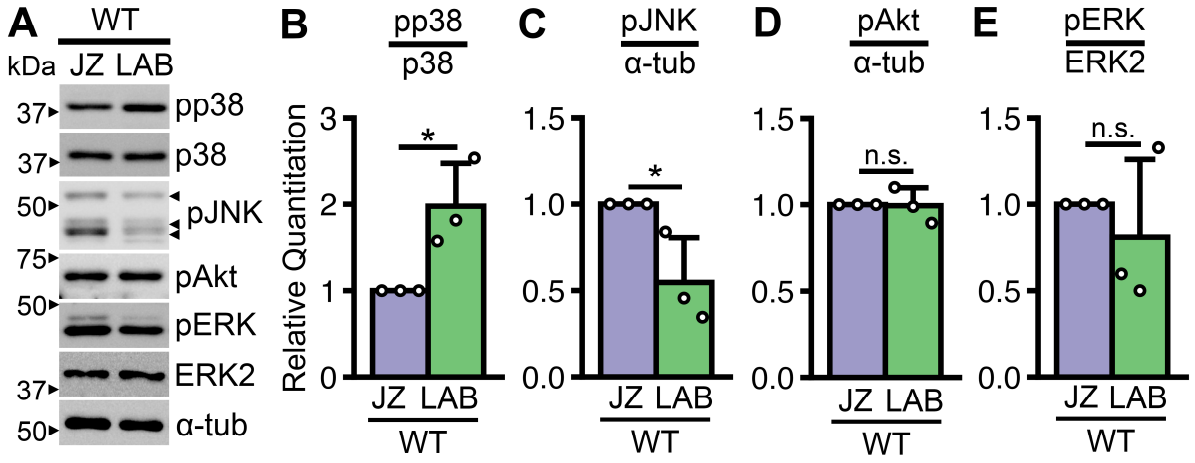


Figure 4. Direct comparison of MAPK and Akt signaling pathways in JZ and LAB trophoblasts differentiated for 4 days. (**A**) LAB^{WT} cells exhibited both enhanced p38 activity and reduced JNK activity relative to JZ^{WT} cells. Representative Western blots and (**B**–**E**) densitometry were used to quantify the mean ± SD of $n = 3$ biologically independent experiments. Normalization was performed as indicated, where the target proteins are shown as the numerator and the loading controls are displayed as the denominator. Each point indicates one biologically independent experiment. The p-value thresholds for Student's t-tests are indicated with the following symbols: * [$p < 0.05$] and n.s. [$p > 0.05$].

2.5. MAP3K4 Kinase Activity Impacts Expression of Hspb1 and Hspb8 Transcripts and HSP27 and HSP22 Proteins in TS Cells

In TS cells, MAP3K4 has been shown to control histone acetylation and gene expression through CBP/p300 and HDAC6 [10,11,17,18]. To assess MAP3K4-dependent gene expression in TS cells, RNA sequencing (RNA-seq) data were used to examine differentially expressed genes (DEGs) in TS^{WT} and TS^{KI} cells (Table S2) [11,18]. We found 1438 genes were significantly increased in TS^{KI} cells relative to TS^{WT} cells, while 1481 genes were significantly decreased in TS^{KI} cells compared to TS^{WT} cells (Figure 5A,B, Tables S3 and S4). Interestingly, *Hspb8* was the most significantly decreased gene (Figure 5A,B). Due to these findings, we wondered if expression of other HSP genes was altered by MAP3K4 in TS cells. Our RNA-seq data were used to examine HSP gene expression levels in TS cells and showed high expression of *Hspb1* and *Hspb8*, which encode HSP27 and HSP22, respectively, in these cells (Table 1). *Hspb8* expression was significantly decreased in TS^{KI} cells when compared to TS^{WT} cells, while *Hspb1* expression was modestly decreased (Table 1). qPCR was performed using primers for *Hspb1* and *Hspb8* and showed both transcripts were significantly decreased in TS^{KI} cells when compared to TS^{WT} cells (Figure 5C). Western blot and densitometry data indicated HSP27 and HSP22 expression was significantly decreased in TS^{KI} cells relative to TS^{WT} cells (Figure 5D,E). The ratio of decreased *Hspb1* transcript to decreased HSP27 protein in TS^{KI} cells relative to TS^{WT} cells was 2.387, suggesting more significant loss of HSP27 protein expression compared to transcript in TS^{KI} cells (Table S5). pHSP27 was also significantly decreased when normalized to total HSP27, showing dependence of pHSP27 levels on upstream signaling pathways in TS cells (c.f. Figures 1A and 5D and Table S6). Overall, our findings demonstrate that MAP3K4 kinase activity in TS cells impacts the expression of HSP27 and HSP22 at both the transcript and protein levels.

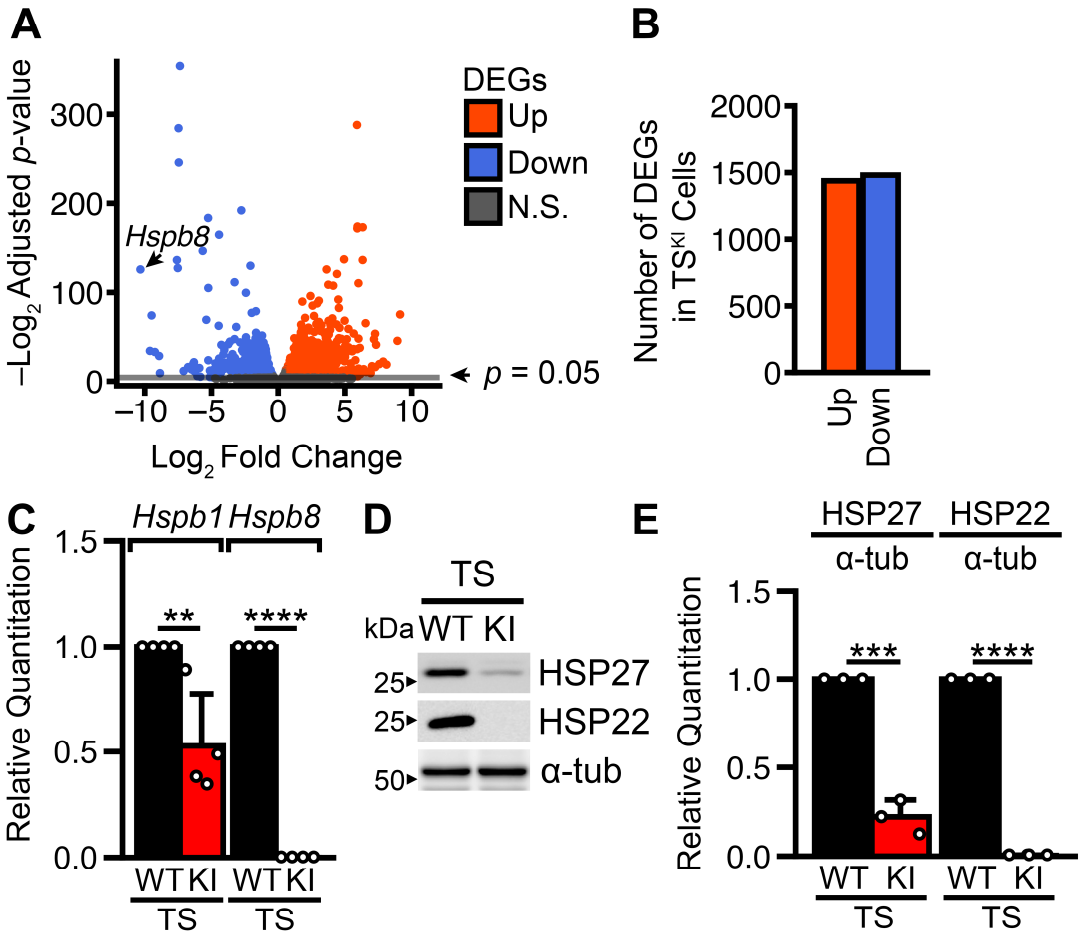


Figure 5. *Hspb1* and *Hspb8* transcript expression and HSP27 and heat shock protein 22 (HSP22) protein expression are reduced in TS cells lacking MAP3K4 kinase activity. (**A**,**B**) DESeq2 analyses performed on RNA sequencing (RNA-seq) data show TS^{KI} cells exhibit both up- and downregulation of differentially expressed genes (DEGs) relative to TS^{WT} cells. (**C**) *Hspb1* and *Hspb8* are reduced in TS^{KI} cells relative to TS^{WT} cells. Quantitative PCR (qPCR) data normalized to *Gapdh* are expressed as a fold-change relative to TS^{WT} cells and represent the mean ± SD of $n = 4$ biologically independent experiments. (**D**) HSP27 and HSP22 levels decreased in TS^{KI} cells relative to TS^{WT} cells. Representative Western blots and (**E**) densitometry were used to quantify the mean ± SD of $n = 3$ biologically independent experiments. HSP27 and HSP22 were normalized to α-tub. Each point indicates one biologically independent experiment. (**C**,**E**) The *p*-value thresholds for Student's *t*-tests are indicated with the following symbols: ** [$p < 0.01$], *** [$p < 0.001$], and **** [$p < 0.0001$].

Table 1. MAP3K4 promotes the transcript expression of specific small HSPs in TS cells.

Gene	TS^{WT} Mean RPKM	TS^{KI} Mean RPKM	Log2 FC [b]	*p*-Value [b]	Result
Hspb1 [a]	67.723	58.919	−0.320	0.5915	n.s.
Hspb2	1.444	0.594	−1.428	0.2586	n.s.
Hspb3	0.000	0.000	NA	NA	n.s.
Hspb6	0.842	1.091	0.253	0.6818	n.s.
Hspb7	0.352	0.355	−0.112	NA	n.s.
Hspb8 [a]	16.995	0.011	−10.328	<0.0001	****
Hspb9	0.191	0.138	−0.589	0.8125	n.s.
Hspb11	1.397	1.414	NA	NA	n.s.

[a] Genes meeting the threshold of greater than two reads per kilobase of transcript per million mapped reads (RPKM) in TS^{WT} or TS^{KI} cells. [b] Log2 FC values and BH-adjusted *p*-values were calculated by using mapped counts and the DESeq2 R package. The *p*-value thresholds for Wald tests are indicated with the following symbols: **** [$p < 0.0001$], n.s. [$p > 0.05$], and NA [not available].

2.6. Expression of HSP27 and HSP22 Is Induced by Differentiation of TS Cells to JZ and LAB Trophoblasts

Since we found HSP27 and HSP22 were both highly expressed in TS cells that form the placenta, we wondered if trophoblast differentiation leads to changes in HSP expression. To examine these proteins in differentiated trophoblasts, we performed Western blotting on TS^{WT} cells differentiated to JZ^{WT} trophoblasts, finding increased pHSP27, HSP27, and HSP22 expression (Figure 6A). Differentiation of TS^{WT} cells to LAB^{WT} trophoblasts led to increased and sustained pHSP27 and HSP27 expression; however, induction of HSP22 was transient (Figure 6B). Densitometry revealed statistical significance of induction of HSPs through JZ^{WT} and LAB^{WT} differentiation, while pHSP27 normalized to total HSP27 was higher in these cells (Figure 6C and Table S6). To directly determine if pHSP27, HSP27, and HSP22 were differentially expressed between JZ^{WT} and LAB^{WT} cells, we compared expression of these proteins between 4-day differentiated JZ^{WT} and LAB^{WT} trophoblasts. HSP27 was significantly higher in JZ^{WT} cells compared to LAB^{WT} cells, whereas HSP22 expression was similar (Figure 6D,E). Interestingly, even though total HSP27 levels were lower in LAB^{WT} cells, pHSP27 was higher in LAB^{WT} cells relative to JZ^{WT} cells (Figure 6D,F and Table S6). qPCR measuring *Hspb1* and *Hspb8* expression showed both transcripts were induced by 4-day differentiation of TS cells to JZ and LAB trophoblasts (Figure 6G). *Hspb1* transcript was higher in JZ^{WT} cells relative to LAB^{WT} cells, but did not reach statistical significance ($p = 0.06$) (Figure 6G). In contrast, *Hspb8* expression was similar between JZ^{WT} and LAB^{WT} cells (Figure 6G). We mined a published microarray dataset of TS cells differentiated to LAB trophoblasts for *Hspb1* and *Hspb8* expression, finding these transcripts were significantly increased throughout LAB differentiation in this dataset (Figure 6H) [35]. Altogether, our data show HSP27 and HSP22 transcript and protein expression are induced by in vitro trophoblast differentiation, and HSP27 is enriched in JZ cells, while pHSP27 is higher in LAB cells.

In vivo differentiation of TS cells leads to formation of the trophoblasts found within the LAB and JZ regions of the placenta (Figure S1) [1,2,5,6,33,34]. TS cells originate from the trophectoderm of embryonic day 3.5 (E3.5) blastocysts; by E9.5, most TS cells have differentiated to form trophoblast progenitors and some mature trophoblasts with JZ characteristics [33,34,36]. The mature trophoblasts of the LAB have not formed at E9.5. In contrast, the E14.5 placenta has a relatively small population of trophoblast progenitors and a large number of mature JZ and LAB trophoblasts. These characteristics make the E9.5–E14.5 developmental timeframe a model for in vivo trophoblast differentiation and placentation [1,2,33,34,36]. Due to our new findings using in vitro differentiation of stem cells, we wanted to examine these pathways using placental tissue. However, unlike the isolation of protein from cultured cells, protein extraction from placental tissues required the use of radioimmunoprecipitation assay (RIPA) buffer containing sodium dodecyl sulfate and sodium deoxycholate. We found that RIPA extracted protein lysis disrupted the ability of anti-phospho-p38 and anti-phospho-JNK antibodies to recognize their targets. Thus, we focused on changes in the expression and phosphorylation of the heat shock proteins during development in vivo. Western blotting and densitometry performed on male and female, sex-matched E9.5, E10.5, E12.5, E13.5, and E14.5 placentas showed that pHSP27 and total HSP27 significantly increased as gestational age (GA) increased (Figure 6I–K). Surprisingly, HSP22 expression significantly decreased as GA increased (Figure 6I,L). Furthermore, our data suggested a correlation between placental sex and HSP27 expression, where male placentas expressed significantly higher levels of HSP27 ($p < 0.05$) when compared to female placentas (Figure 6K). Overall, our in vivo and in vitro findings regarding HSP27 were concordant and showed enhanced HSP27 expression and phosphorylation throughout trophoblast differentiation.

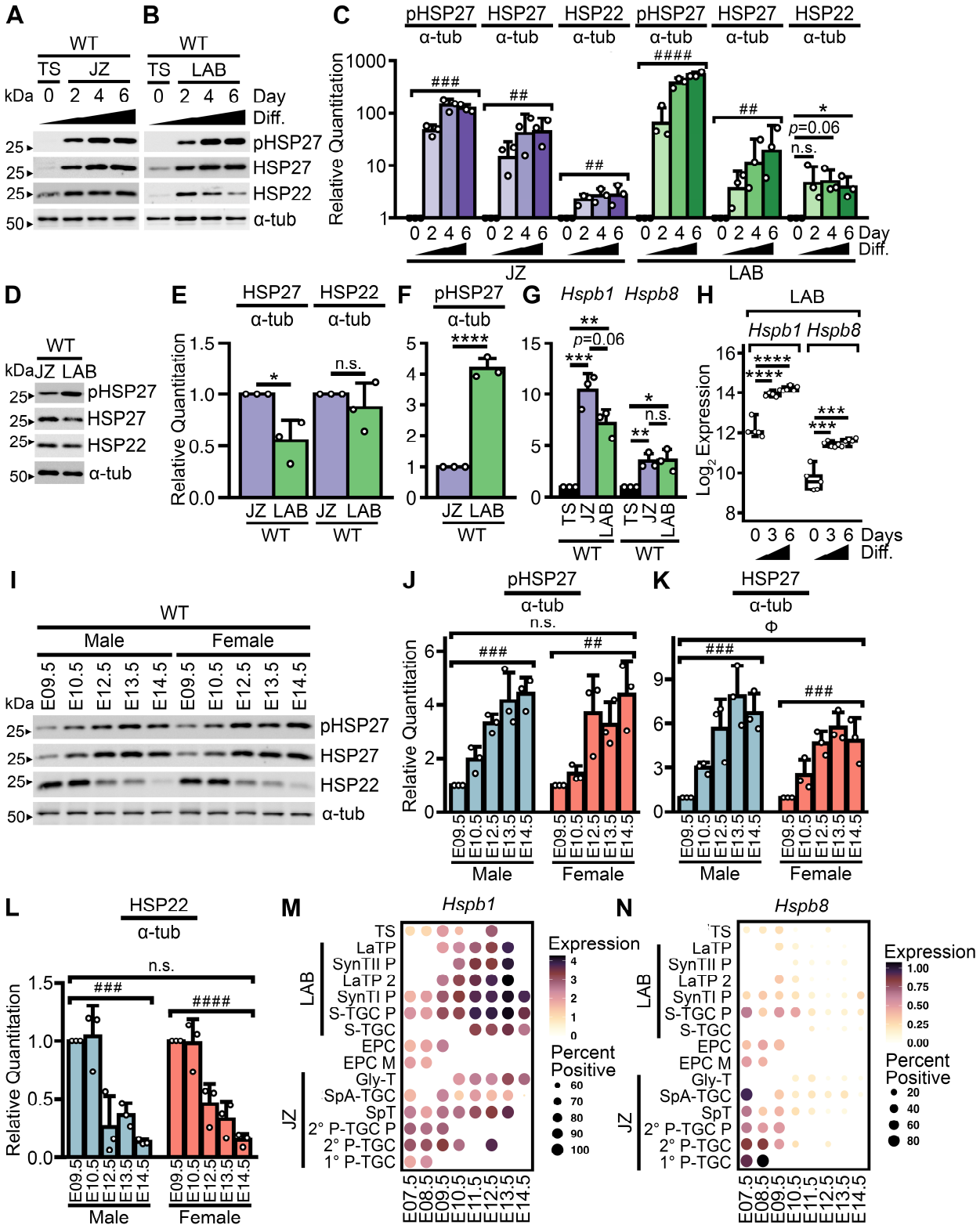


Figure 6. Differential induction of phosphorylated HSP27, total HSP27, and total HSP22 during TS cell formation of the labyrinth versus the junctional zone. (**A**–**C**) Trophoblast differentiation results in increased pHSP27, HSP27, and HSP22 expression. (**D**–**F**) pHSP27 is increased and HSP27 is reduced in LAB^{WT} cells relative to JZ^{WT} cells differentiated for four days. (**D**) and Figure 4A show images from the same biological sample set and share the same α-tub blot used as a loading control. (**G**) *Hspb1* and *Hspb8* are induced when TS^{WT} cells are differentiated to JZ^{WT} and LAB^{WT} cells for four days. qPCR data normalized to *Gapdh* are the mean ± SD of $n = 3$ biologically independent experiments. (**H**) Microarray data from GSE266153 were mined to show *Hspb1* and *Hspb8* expression

during in vitro TS^{WT} cell differentiation to LAB^{WT} trophoblasts. (**I**–**L**) In vivo placental development induces pHSP27 and HSP27 while HSP22 expression is decreased during gestation. (**M**,**N**) Single-cell RNA-seq data from GSE156125 were mined, showing increasing *Hspb1* expression and decreasing *Hspb8* expression during in vivo placental development. (**A**,**B**,**D**,**I**) Representative Western blots and (**C**,**E**,**F**,**J**–**L**) densitometry were used to quantify the mean ± SD of $n = 3$ biologically independent experiments. Expression of pHSP27, HSP27, and HSP22 were normalized to α-tub. For all graphs, each point represents one biologically independent sample. (**C**,**E**–**H**) The *p*-value thresholds for Student's *t*-tests are indicated with the following symbols: * [$p < 0.05$], ** [$p < 0.01$], *** [$p < 0.001$], **** [$p < 0.0001$], and n.s. [$p > 0.05$]. (**C**,**J**–**L**) The *p*-value thresholds for one-way ANOVA are indicated with the following symbols: ## [$p < 0.01$], ### [$p < 0.001$], #### [$p < 0.0001$]. (**J**–**L**) The *p*-value thresholds for two-way ANOVA are indicated with the following symbols: Φ [$p < 0.05$] and n.s. [$p > 0.05$]. Undefined acronyms: E (embryonic day), ectoplacental cone (EPC), EPC migratory cell (EPC M), glycogen trophoblast (Gly-T), LAB trophoblast progenitor (LaTP), primary parietal-trophoblast giant cell (1° P-TGC), secondary P-TGC (2° P-TGC), secondary P-TGC precursor (2° P-TGC P), spiral artery-trophoblast giant cell (SpA-TGC), spongiotrophoblast (SpT), sinusoidal-trophoblast giant cell (S-TGC), S-TGC precursor (S-TGC P), syncytiotrophoblast I precursor (SynTI P), and syncytiotrophoblast II precursor (SynTII P).

Placental tissue is highly heterogeneous, being composed of multiple different cell types in different regions in the JZ and LAB. This complexity makes it difficult to assign the observed protein expression and phosphorylation differences to a single cell population. To partially address this issue, we mined single cell RNA-seq data for *Hspb1* and *Hspb8* expression in a murine placental time course from Jiang et al. [34]. Similar to our Western blotting results from RIPA lysis of placentas at different stages, *Hspb1* expression increased during placental development across most placental cell types, whereas *Hspb8* was highest in the JZ cells early in placental development and decreased to low levels by E11.5 (Figure 6M,N). Together, these data suggest that *Hspb8* may play roles early in placental development, whereas *Hspb1* may be important during mid-gestation.

2.7. MAP3K4 Impacts Hspb1 and Hspb8 Transcripts and HSP27 and HSP22 Protein Expression in Differentiated Trophoblasts

Since MAP3K4 kinase activity was associated with pHSP27, HSP27, and HSP22 expression in TS cells, we wondered if MAP3K4 impacts these proteins in 4-day differentiated JZ and LAB trophoblasts. To address this question, we performed qPCR to measure transcript expression of *Hspb1* and *Hspb8* in JZ^{WT} and JZ^{KI} trophoblasts, finding *Hspb8* expression was significantly decreased in JZ^{KI} trophoblasts relative to JZ^{WT} cells, while expression of *Hspb1* was unchanged (Figure 7A). Our Western blot and densitometry findings were concordant with transcript data and showed expression of HSP22 was significantly decreased and HSP27 was unchanged in JZ^{KI} cells when compared to JZ^{WT} cells (Figure 7B,C). These data suggest loss of HSP22 protein in the absence of MAP3K4 activity is due to loss of *Hspb8* gene expression. Interestingly, although total *Hspb1* and HSP27 were not affected in JZ^{KI} cells, pHSP27 levels were drastically reduced, which is consistent with our findings that showed diminished p38 activity in JZ^{KI} cells (c.f. Figures 2G and 7A–C, and Table S6). In contrast to these findings in JZ^{KI} cells, we discovered through qPCR that both *Hspb1* and *Hspb8* expression were significantly decreased in LAB^{KI} cells compared to LAB^{WT} cells (Figure 7D). Western blot and densitometry data showed the same pattern, where HSP27 and HSP22 expression were significantly decreased in LAB^{KI} cells relative to LAB^{WT} cells (Figure 7E,F). Further, pHSP27 was also significantly decreased in LAB^{KI} cells, indicating that reduced p38 activity as well as reduced *Hspb1* transcript and HSP27 protein expression were responsible for lowered pHSP27 levels in these cells (c.f. Figures 3G and 7D–F, and Table S6). Together, our findings suggest potential roles of MAP3K4 for activation of signaling pathways and the expression of heat shock proteins in differentiated trophoblasts.

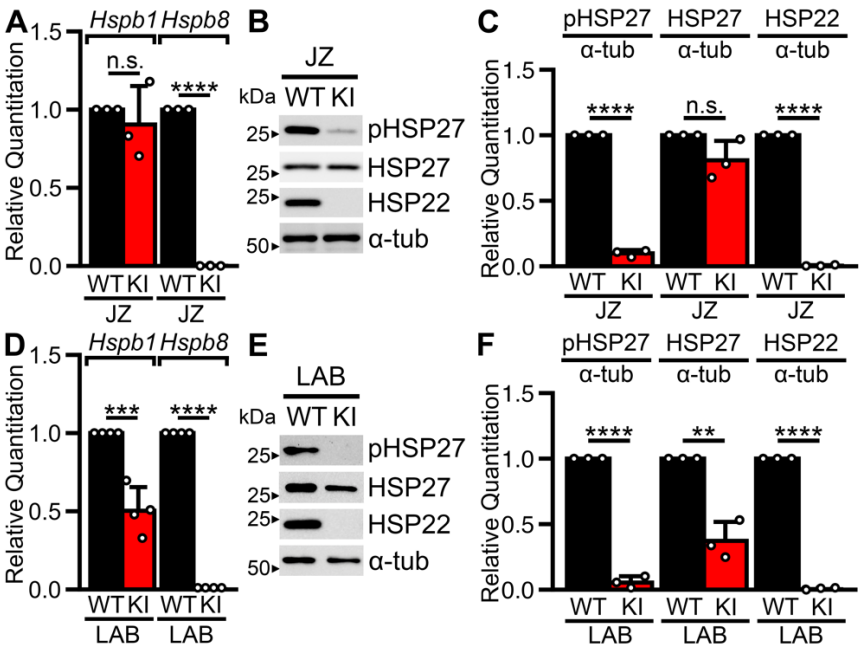


Figure 7. Loss of MAP3K4 kinase activity in differentiated trophoblasts impairs HSP22 expression and HSP27 phosphorylation. (**A**) *Hspb8* is reduced in JZ^{KI} cells relative to JZ^{WT} cells. (**B**,**C**) pHSP27 and HSP22 are decreased in JZ^{KI} cells relative to JZ^{WT} cells. (**D**) *Hspb1* and *Hspb8* are reduced in LAB^{KI} cells relative to LAB^{WT} cells. (**E**,**F**) pHSP27, HSP27, and HSP22 are decreased in LAB^{KI} cells relative to LAB^{WT} cells. (**A**,**D**) qPCR data normalized to *Gapdh* are the mean ± SD of (**A**) $n = 3$ and (**D**) $n = 4$ biologically independent experiments. (**B**,**E**) Representative Western blots and (**C**,**F**) densitometry were used to quantify the mean ± SD of $n = 3$ biologically independent experiments. Expression of pHSP27, HSP27, and HSP22 were normalized to α-tub. Each point indicates one biologically independent experiment. (**A**,**C**,**D**,**F**) The *p*-value thresholds for Student's *t*-tests are indicated with the following symbols: ** [$p < 0.01$], *** [$p < 0.001$], **** [$p < 0.0001$], and n.s. [$p > 0.05$].

2.8. Re-Expression of the MAP3K4/CBP/HDAC6 Coregulated Gene Rel in TS^{KI} Cells Promotes Hspb1 and Hspb8 Transcript Expression

A key question to be addressed was related to the potential indirect versus direct mechanism(s) by which MAP3K4 impacts gene expression of *Hspb1* and *Hspb8*. We have previously shown that MAP3K4 directly controls expression of select genes by promoting the activity of the histone acetyltransferase CBP and inhibiting the expression and activity of the histone deacetylase HDAC6. MAP3K4 activates JNK and p38, which phosphorylate CBP [10]. Now active, phosphorylated CBP acetylates histone H2B on Lysine 5 (H2BK5Ac) on specific genes [10]. MAP3K4 physically binds to HDAC6, inhibiting its activity and promoting its ubiquitination and degradation [11,17]. KI MAP3K4 binds HDAC6 but fails to promote its degradation, resulting in increased HDAC6 in the cytoplasm and nucleus. Nuclear HDAC6 binds to select genes, deacetylating H2BK5Ac and repressing the expression of these genes. Some MAP3K4 regulated genes are controlled by either CBP or HDAC6. We recently discovered that some genes are co-regulated, meaning transcript expression of the gene is both activated by CBP and inhibited by HDAC6. One of these co-regulated genes is the NF-kB family member *Rel* [18]. Others have published that NF-kB promotes the expression of *Hspb8* [37–39]. We analyzed our previously published H2BK5Ac chromatin immunoprecipitation (ChIP)-seq data finding that acetylation of the *Hspb1* and *Hspb8* promoters was reduced by 67.3% ($p < 0.0001$) and 86.5% ($p = 0.00123$) respectively in TS^{KI} cells relative to TS^{WT} cells [10]. Analyses of our published microarray data comparing gene expression in TS^{KI} cells to TS^{KI} cells re-expressing REL showed dramatic changes in gene expression induced by re-expression of REL (Figure 8A,B). *Hspb1* and *Hspb8* transcript expression increased with REL re-expression in TS^{KI} cells (Figure 8C,D). These data provide

a possible direct mechanism from MAP3K4 signaling to promote REL expression to the expression of *Hspb1* and *Hspb8* genes through MAP3K4 control of histone modifiers and key transcription factors.

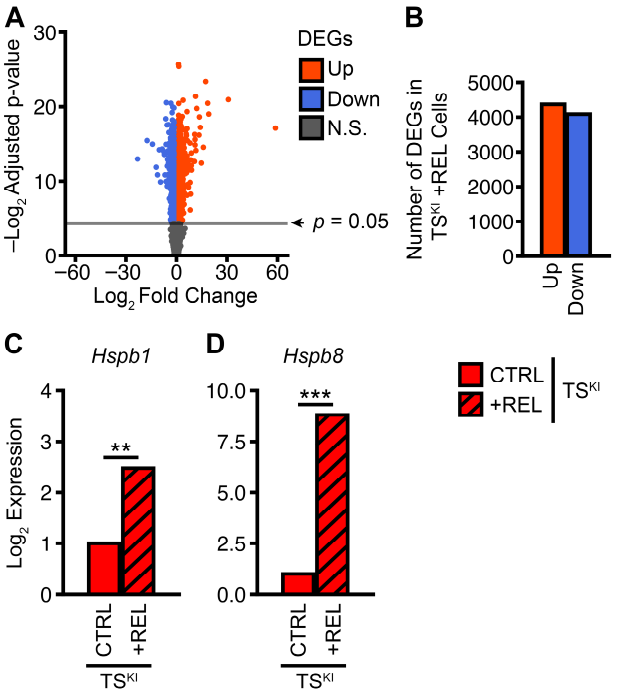


Figure 8. Re-expression of REL in TS^{KI} cells leads to increased *Hspb1* and *Hspb8* expression. Microarray data from GSE148250 were mined (**A**,**B**) showing increased and decreased DEGs when REL is re-expressed in TS^{KI} (+REL) cells relative to control TS^{KI} (CTRL) cells. (**C**,**D**) Expression of both *Hspb1* and *Hspb8* are significantly increased in TS^{KI} +REL cells when compared to TS^{KI} CTRL cells. The *p*-value thresholds for Student's *t*-tests are indicated with the following symbols: ** [$p < 0.01$], and *** [$p < 0.001$]. All panels represent microarray data from $n = 3$ biologically independent samples.

2.9. Autophagic Flux Is Disrupted in KI Cells That Have Reduced Expression of Regulators of Autophagy, Hspb1, and Hspb8

Our new data showed reduced expression of *Hspb1*/HSP27 and *Hspb8*/HSP22 in the absence of MAP3K4 kinase activity in TS cells and differentiated trophoblasts. Small HSPs can act as holdases to prevent substrate aggregation and can assist in the refolding of substrates [26]. In addition, small HSPs can promote substrate degradation through the proteosome and autophagosome–lysosome [26]. Interestingly, HSP27 and HSP22 can heterodimerize, and both promote proteostasis, including autophagy [26,40–42]. Autophagy is a catabolic process where intracellular material including damaged organelles and protein aggregates are engulfed by double-membrane autophagosomes. Fusion with lysosomes leads to degradation of the cellular material that can be recycled. Autophagy in the placenta is critical to normal function and disruption is associated with diseases of pregnancy [43–45]. Deletion of select autophagy related genes such as *Atg7* in mice results in reduced placental function and fetal growth restriction similar to *Map3k4*$^{KI/KI}$ mice [8,46,47]. *Hspb1*/HSP27 binds to the autophagy receptor SQSTM1/p62 to promote autophagy [27]. *Hspb8*/HSP22 interacts with BAG3 to promote chaperone assisted selective autophagy (CASA) [26,37,41,42]. Both mouse and human placental development increase autophagic flux [43,45,46,48–50]. Based on the well-defined roles for HSP27 and HSP22 in autophagy, we examined autophagic flux by inhibiting the fusion of autophagosomes with lysosomes using chloroquine and performing immunofluorescence staining for GABA type A receptor-associated protein (GABARAP), a positive marker of autophagosomes [51]. GABARAP fluorescence was diffuse and weak in both TS^{WT} and TS^{KI} cells (Figure 9A).

Differentiation of TS^{WT} cells to JZ^{WT} cells robustly increased autophagic flux as shown by accumulation of GABARAP in large, perinuclear autophagosomes (Figure 9A). Differentiation to the LAB also induced GABARAP-positive vesicles that were enriched in regions of syncytialization (Figure 9A). Quantification of GABARAP fluorescence per cell showed statistically significant increases in GABARAP fluorescence after differentiation of TS^{WT} cells to form the JZ^{WT} or LAB^{WT} cells (Figure 9B). GABARAP fluorescence was not significantly different between JZ^{WT} or LAB^{WT} cells (Figure 9C). Although basal autophagic flux was slightly decreased in TS^{KI} cells relative to TS^{WT} cells ($p < 0.01$), GABARAP-positive autophagosomes were dramatically reduced in both JZ^{KI} relative to JZ^{WT}, and LAB^{KI} relative to LAB^{WT} ($p < 0.0001$) (Figure 9A,D–F). Altogether, these data suggest roles for MAP3K4, HSP27, and HSP22 in trophoblast responses during cellular differentiation.

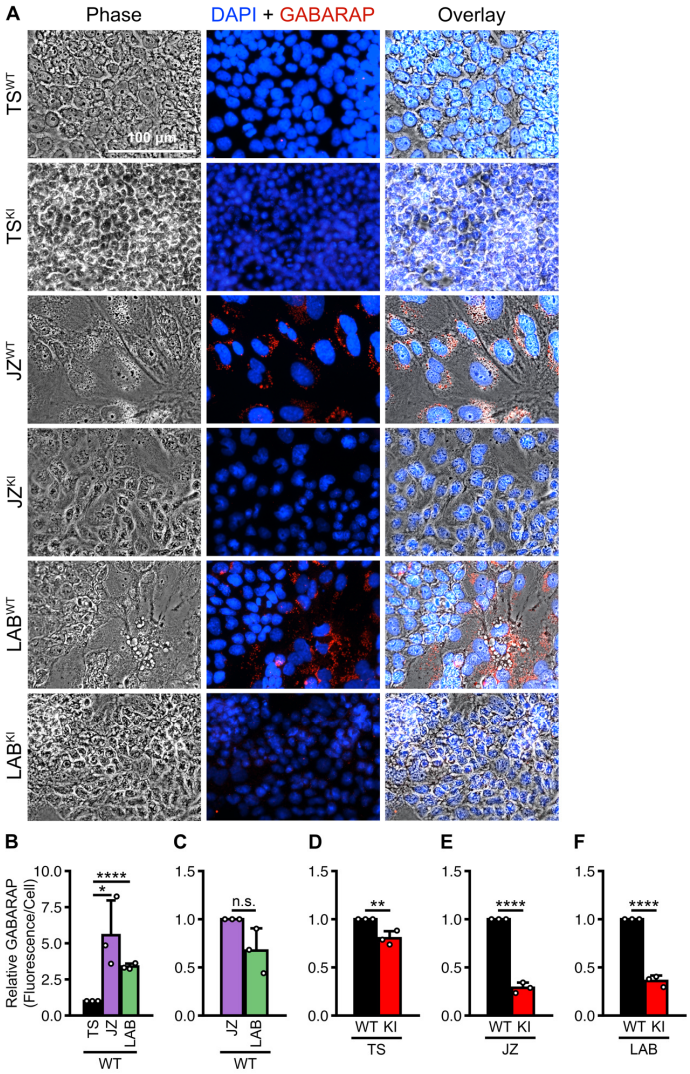


Figure 9. Autophagy is induced by trophoblast differentiation in a MAP3K4-dependent manner. (**A**) The rate of autophagy in TS cells is low; trophoblast differentiation induces GABA type A receptor-associated protein (GABARAP) accumulation in WT cells. (**B**) GABARAP expression levels are significantly increased in JZ^{WT} and LAB^{WT} trophoblasts when compared to TS^{WT} cells. (**C**) Expression of GABARAP between JZ^{WT} and LAB^{WT} trophoblasts is not significantly different. (**D**) GABARAP expression is modestly decreased in TS^{KI} cells when compared to TS^{WT} cells. (**E**,**F**) Levels of GABARAP are significantly decreased in KI differentiated trophoblasts when compared to the WT controls. Each point indicates one biologically independent experiment. (**B**–**F**) The *p*-value thresholds for the Student's *t*-tests are indicated with the following symbols: * [$p < 0.05$], ** [$p < 0.01$], **** [$p < 0.0001$], and n.s. [$p > 0.05$]. All panels represent $n = 3$ biologically independent experiments.

3. Discussion

Herein, we define signaling pathways during TS cell differentiation, showing transient JNK activity during JZ differentiation compared to sustained p38, JNK, and Akt activation during LAB differentiation. Importantly, activation of JNK and p38 in JZ and LAB cells was affected by MAP3K4 activity. We also discovered expression of HSP22 and HSP27, two highly expressed HSPs in TS cells, was robustly induced by TS cell differentiation to JZ and LAB trophoblasts. Surprisingly, when JZ and LAB trophoblasts were directly compared, HSP27 expression was higher in JZ cells, while pHSP27 levels were higher in LAB cells. In both TS and LAB cells, pHSP27, HSP27, and HSP22 expression levels were affected by MAP3K4 kinase activity. MAP3K4 promoted the expression of REL, a NF-kB family member that induced expression of *Hspb1* and *Hspb8*. Loss of MAP3K4 kinase activity and reduced *Hspb1*, and *Hspb8* expression were associated with decreased autophagy that may impact the metabolic state of the developing embryos and placentas. Overall, these data show MAP3K4 may impact expression and activation of HSP proteins involved in proteostasis responses during differentiation of TS cells to form trophoblasts.

In TS cells, MAP3K4 is known to activate p38, JNK, and Akt under basal conditions [6,8,19]. Our new study expands our understanding of these pathways in placental trophoblasts, finding activation of MAP3K4-dependent pathways and HSP expression in these cells. We show JNK is more active in JZ cells and p38 is more active in LAB cells, suggesting roles for these pathways in placental trophoblasts. Surprisingly, pHSP27 increased through JZ differentiation despite no change in p38 activity. This result may be due to increased *Hspb1* transcript and HSP27 protein expression. Although p38-activated MK2 is the primary kinase responsible for phosphorylation of HSP27, several additional kinases including Akt have been shown to directly phosphorylate HSP27 [25,52]. Significantly, Akt phosphorylation increased during JZ differentiation, suggesting Akt may be responsible for some of these changes in pHSP27 in the JZ. Increased pHSP27 during LAB differentiation is consistent with increased HSP27 transcript and protein expression as well as sustained p38 and Akt activation observed during LAB differentiation. When directly compared, JZ trophoblasts exhibited higher HSP27, while pHSP27 was higher in LAB trophoblasts, suggesting a possible role for the HSP27 large oligomer in JZ cells and the pHSP27 small oligomer in LAB cells. Increased small, phosphorylated HSP27 oligomers during LAB trophoblast differentiation may play important roles such as increasing chaperone efficiency and modulation of apoptosis when compared to JZ trophoblasts. HSP22 expression increased through in vitro differentiation and decreased through in vivo differentiation, possibly due to the changes in cell type frequency across in vivo placental development. Further, we found that MAP3K4 KI led to decreased pHSP27 levels when normalized to total HSP27 in placental trophoblasts, indicating a potential increase in large HSP27 oligomers and a decrease in chaperone efficiency in these cells. As described in the results section, the placenta is composed of many cell types in different regions. Our single cell RNA-seq analyses showed selective *Hspb1* and *Hspb8* expression patterns in different cell types. However, these data do not address changes in phosphorylation of HSPs. The MAP3K4-dependent pathways and HSPs have overlapping roles in other systems, including protection against proteotoxicity caused by stress [26,53,54]. We hypothesize that MAP3K4 may facilitate responses to proteotoxic stress in placental trophoblasts. Together, our findings demonstrate potential functions of MAP3K4 in regulation of stress and differentiation during placental development.

While our data suggest normal roles for MAP3K4 in placental trophoblasts, suppression of MAP3K4-dependent pathways and HSPs may lead to the pathologies found in *Map3k4*$^{KI/KI}$ mice. Our lab has shown MAP3K4 KI promotes trophoblast hyperinvasion, placental insufficiency, FGR, and embryonic and perinatal lethality during placental devel-

opment [6,8–10]. Herein, we show MAP3K4 KI leads to diminished MAPK signaling and HSP expression in response to stress and differentiation in placental trophoblasts. Additionally, decreased activation of autophagy is known to result in FGR and miscarriage [43–49]. Cellular stress regulates developmental processes such as trophoblast invasion and differentiation, suggesting impaired trophoblast responses to stress and differentiation stimuli may promote trophoblast hyperinvasion, maintenance of TS cell stemness, FGR, and embryonic and perinatal lethality [6,22,55]. Further, *Mapk14* (p38α) knockout leads to embryonic death, indicating that inhibited p38 activity during development may explain in part the embryonic lethality found in *Map3k4*$^{KI/KI}$ mice [56]. Loss of MAP3K4-dependent signaling and diminished pHSP27, HSP27, and HSP22 expression may be responsible for the pathologies leading to FGR and lethality in humans and mice.

In summary, we have shown p38 and JNK are differentially activated in LAB and JZ trophoblasts, suggesting contrasting roles for these pathways in these cell types. We also discovered p38 and JNK are activated by MAP3K4 in LAB and JZ cells. We found JZ differentiation led to higher levels of total HSP27, whereas LAB differentiation led to increased pHSP27 levels, indicating potential functions for phosphorylated and total HSP27 in JZ and LAB cells. Furthermore, pHSP27, HSP27, and HSP22 levels were all supported by MAP3K4 kinase activity in TS and LAB cells. Our work demonstrates previously unknown roles for MAP3K4 in JZ and LAB trophoblast differentiation during murine placental development. Future studies will examine the impact of suppressed MAP3K4-dependent signaling and reduced HSP22 and HSP27 expression on human and mouse placental trophoblasts, including potential proteostasis-related phenotypes, such as protein aggregation and dysregulated autophagy. Investigations of these functions of MAP3K4 in placental trophoblasts may provide a potential therapeutic target to treat diseases that arise from placental insufficiency, such as FGR.

4. Materials and Methods

4.1. Cell Lines and Culture Conditions

TS^{WT} and TS^{KI} cells were previously isolated from *Map3k4*$^{WT/WT}$ and *Map3k4*$^{KI/KI}$ mouse embryos, respectively [6]. TS cells were cultured as previously described in TS media containing RPMI 1640, 20% heat inactivated fetal bovine serum, 1% penicillin and streptomycin, 1% sodium pyruvate, 1% L-glutamine, and 100 μM β-mercaptoethanol [5,6]. For maintenance of the stem cell state, TS cells were cultured in conditioned TS media (30% TS media and 70% MEF-CM with 37.5 ng/ml FGF4 and 1 μg/ml heparin) [5,6]. To induce osmotic stress, sorbitol was dissolved in RPMI 1640 and added to the conditioned TS media for a final concentration of 181.8 mM, while an equal volume of RPMI 1640 was added to the untreated samples. For the UV treatments, uncovered TS cells were irradiated with 302 nm UV-B light for 1 min using the Bio-Rad ChemiDoc Touch (Bio-Rad, Hercules, CA, USA). Then, the cells were incubated for 1 h at 37 °C before lysis. JZ and LAB trophoblasts were formed through differentiation of TS cells using previously published methods [5–8]. Briefly, TS cells were seeded in conditioned TS media with FGF4 and Heparin. Differentiation of TS cells for two days was performed by removing the conditioned TS media after 48 h, followed by the addition of TS media only; 4- and 6-day TS cell differentiation occurred through the replacement of the conditioned TS media with TS media alone after 24 h. Differentiation of TS cells to JZ trophoblasts used TS media alone, while differentiation of TS cells to LAB trophoblasts required TS media with 3 μM CHIR99021 (Selleck Chemicals, Houston, TX, USA) added daily [7]. The 4-day differentiation time point was used for experiments directly comparing JZ^{WT} and LAB^{WT}, JZ^{WT} and JZ^{KI}, or LAB^{WT} and LAB^{KI} samples. For assessments of autophagic

flux, cells were treated for 16 h with 50 μM chloroquine to inhibit the fusion of late stage autophagosomes with lysosomes [57].

4.2. Mouse Models and Dissections

All experimental samples were isolated from mice in a pure 129/SvEv background. For all placenta dissections, mice were checked each morning for a copulatory plug, and noon of the day detected was considered E0.5. Pregnant females were euthanized at E9.5, E10.5, E12.5, E13.5, and E14.5, and the embryos and placentas were isolated. Embryonic material was used for sex genotyping, and placentas were used for protein extraction.

4.3. Protein Extraction, SDS-PAGE, Western Blotting, and Densitometry

Whole-cell lysates of TS cells were extracted as previously described [6,9]. Briefly, whole-cell lysates were harvested using buffer A (20 mM Tris [pH 7.4], 150 mM NaCl, 1 mM EDTA, 1 mM EGTA, and 1% Triton X-100) with phosphatase and protease inhibitors [12,16]. Due to inefficient lysis of placental tissue using Buffer A alone, protein was extracted from placental tissue by homogenizing each placenta for 5 s on ice in RIPA buffer (buffer A, 0.1 mg/ml SDS, and 0.1 mg/ml sodium deoxycholate) with phosphatase and protease inhibitors [8]. The placental lysates remained on ice for 10 min while vortexing the lysates every 2.5 min. Then, the lysates were spun at 16,200× *g* for 10 min at 4 °C. Bradford assays were performed to measure protein concentration. SDS-PAGE was performed to resolve proteins, and proteins were transferred to nitrocellulose membranes, which were blotted with the indicated antibodies as shown in Table S7. Western blots were imaged using Bio-Rad Clarity Western ECL Substrate and a Bio-Rad ChemiDoc Touch (Bio-Rad, Hercules, CA, USA). Densitometry was performed using Bio-Rad Image Lab software Version 5.2.1. Densitometry was normalized as shown in each figure, where the value for the target protein (shown in the numerator) was divided by the value for the loading control (shown in the denominator) for each sample. Relative fold-change values were calculated by dividing the normalized densitometry values by the control. According to the manufacturer (Cell Signaling Technology, Danvers, MA, USA), the anti-phospho JNK antibody may also cross-react with phosphorylated p38 and ERK, and it may recognize JNK when singly phosphorylated.

4.4. Sex Genotyping

Genotyping of sex chromosomes was performed as previously described [16]. Briefly, genomic DNA was isolated from whole embryos (E9.5 and E10.5) or embryonic tail snips (E12.5, E13.5, and E14.5). Sex genotyping was accomplished through PCR and primers that amplify *Ube1y1* and *Ube1x* genes simultaneously. Primers for each gene are shown in Table S8.

4.5. RNA Processing and qPCR

RNA was isolated from TS cells using the RNeasy Plus mini kit (Qiagen, Hilden, Germany). Complementary DNA was generated from 3 μg of RNA using the High-Capacity cDNA Reverse Transcription Kit (Thermo Fisher Scientific, Waltham, MA, USA). Gene expression changes were measured using the Bio-Rad CFX96 Touch (Bio-Rad, Hercules, CA, USA) along with iTaq (Bio-Rad, Hercules, CA, USA). Each biologically independent RNA sample was measured using three technical replicates that were averaged by the Bio-Rad CFX Maestro software version 4.0.2325.2 and CFX Manager software Version 3 to calculate the value for a biologically independent sample. A minimum of three biologically independent samples were measured. Changes in gene expression were normalized to *Gapdh* as indicated in the figure legends. Primers for each gene are shown in Table S8.

4.6. RNA Sequencing and Analysis

RNA sequencing (RNA-seq) was performed on TS^{WT} and TS^{KI} cells as previously described [11,18]. RNA-seq data sets were processed and differentially expressed genes (DEGs) were identified with the DESeq2 (Version 1.44.0) package in R (4.4.1) and R studio (2025.09.2+418) [58]. More information about the datasets used in this study can be found in Table S2. The increased and decreased DEGs in TS^{KI} cells relative to TS^{WT} cells can be found in Table S3 and Table S4, respectively.

4.7. Statistics, Data Analysis, and Figure Generation

Statistical analyses were performed using R, R studio, tidyverse (2.0.0), DESeq2, and Microsoft Excel (16.56) [58,59]. Densitometry of Western blots and qPCR were analyzed using two-tailed unpaired Student's *t*-test, one-way ANOVA, and two-way ANOVA as indicated in the figure legend. The Wald test for DEGs and Benjamini–Hochberg (BH) *p*-value adjustments were performed on TS^{WT} and TS^{KI} cell RNA-seq data sets by using the DESeq2 R package [58]. The microarray datasets GSE266153 measuring in vitro LAB differentiation and GSE148250 measuring TS^{KI} cells re-expressing REL were accessed through GEO [18,35]. More details on all RNA-seq and microarray datasets used in this study can be found in Table S2. Information about the statistical methods used for all experiments including the number of individuals or replicates is defined in each figure legend. The *p*-value thresholds for Student's *t*-tests are indicated with the following symbols: * [$p < 0.05$], ** [$p < 0.01$], *** [$p < 0.001$], **** [$p < 0.0001$], and n.s. [$p > 0.05$]. The *p*-value thresholds for one-way ANOVA tests are indicated with the following symbols: # [$p < 0.05$], ## [$p < 0.01$], ### [$p < 0.001$], #### [$p < 0.0001$], and n.s. [$p > 0.05$]. The *p*-value thresholds for two-way ANOVA tests are indicated with the following symbols: Φ [$p < 0.05$], ΦΦ [$p < 0.01$], ΦΦΦ [$p < 0.001$], ΦΦΦΦ [$p < 0.0001$], and n.s. [$p > 0.05$]. Figures were generated using R, R studio, tidyverse, and Adobe Photoshop [59]. All untrimmed images of Western blots shown herein are included in Figure S2.

4.8. Immunofluorescence and Quantitation

Immunofluorescence assays were performed by aspirating the culture media and washing the cells with PBS. Next, cells were fixed with ice cold 100% methanol and incubated for 15 min at −20 °C. The coverslips were washed three times with PBS and blocked with 5% FBS and 0.3% Triton X-100 in PBS for 1 h at room temperature. Then, the coverslips were washed with PBS and incubated overnight with 1:400 anti-GABARAP antibody (Table S7) in PBS containing BSA and 0.3% Triton X-100 at 4 °C. On the subsequent day, the coverslips were washed three times with PBS over 30 min and incubated with 1:500 AlexaFluor 594 anti-rabbit antibody (Table S7) and 4′,6-diamidino-2-phenylindole (DAPI) (200 ng/mL) in 5% FBS in PBS for 1 h at room temperature. Finally, the cells were washed three times with 0.1% BSA in PBS over 30 min, mounted on slides, and imaged using a BioTek Lionheart FX (Agilent, Santa Clara, CA, USA). Five regions of interest (ROIs) were identified and imaged per biologically independent sample. For selection of ROIs, fields were initially identified using phase imaging, followed by imaging of DAPI (blue) and GABARAP (red) channels. Quantification of fluorescence was performed through the Lionheart FX software Gen5 Version 3. Fluorescence values were normalized by dividing the fluorescence signal by the number of cells present. Then, relative fold-change values were calculated by dividing the mean of the five normalized fluorescence values per sample by the average control value.

Supplementary Materials: The following supporting information can be downloaded at: https://www.mdpi.com/article/10.3390/kinasesphosphatases4020015/s1, Table S1: RNA-seq performed on TS^{WT} and TS^{KI} cells shows ERK2, JNK2, and p38α are the predominantly expressed ERK, JNK,

and p38 proteins in TS cells; Table S2: List of resources used in this study; Table S3: TSKI increased DEGs; Table S4: TSKI decreased DEGs; Table S5: qPCR and densitometry fold-change values were used to calculate the ratio of transcript to protein; Table S6: Densitometry analyses indicate pHSP27 levels are controlled by upstream regulators; Table S7: List of all antibodies used for Western blotting and immunofluorescence experiments; Table S8: List of all primers used for genotyping and qPCR experiments; Figure S1: Differentiation of TS cells leads to the formation of JZ and LAB trophoblasts; Figure S2: Untrimmed Western blot images. References [11,18,34,35] are cited in the Supplementary Materials.

Author Contributions: Conceptualization, N.A.M., P.A.R. and A.N.A.; methodology, N.A.M., P.A.R. and A.N.A.; software, N.A.M.; validation, N.A.M. and A.T.S.; formal analysis, N.A.M.; investigation, N.A.M. and A.T.S.; resources, N.A.M., P.A.R. and A.N.A.; data curation, N.A.M.; writing—original draft preparation, N.A.M. and A.N.A.; writing—review and editing, N.A.M., P.A.R., A.T.S. and A.N.A.; visualization, N.A.M.; supervision, N.A.M. and A.N.A.; project administration, N.A.M. and A.N.A.; funding acquisition, A.N.A. All authors have read and agreed to the published version of the manuscript.

Funding: This research was funded by [National Institute of General Medical Sciences], grant number [GM116903], [National Institute of Child Health and Human Development], grant number [HD113870], and a grant from the University of Memphis College of Arts and Sciences Research Grant Fund.

Institutional Review Board Statement: All experiments using animals were approved by the Institutional Animal Care and Use Committee at the University of Memphis, protocol number [CY23-010] approved on 16 August 2023. All experiments using animals were performed according to institutional and National Institutes of Health guidelines and regulations.

Informed Consent Statement: Not applicable.

Data Availability Statement: The original, non-RNA-seq-related contributions shown in this study are included in the article/Supplementary Data. The GEO accession numbers for all RNA-seq and microarray datasets are shown in Table S2. DESeq2 results for increased and decreased DEGs in TS^{KI} cells are shown in Table S3 and S4. Additional data can be requested by contacting the corresponding author.

Conflicts of Interest: The authors declare no conflicts of interest.

Abbreviations

The following abbreviations are used in this manuscript:

ANOVA	Analysis of variance
α-tub	α-tubulin
BH	Benjamini-Hochberg
ChIP-seq	Chromatin immunoprecipitation-sequencing
DAPI	4′,6-diamidino-2-phenylindole
DEG	Differentially expressed gene
E	Embryonic day
EDTA	Ethylenediaminetetraacetic acid
EGTA	Ethylene glycol-bis(2-aminoethylether)-N,N,N′,N′-tetraacetic acid
EMT	Epithelial-to-mesenchymal transition
ERK	Extracellular signal-regulated kinase
EPC	Ectoplacental cone
EPC M	Ectoplacental cone migratory cell
FC	Fold-change
FGF4	Fibroblast growth factor 4
FGFR1/2	Fibroblast growth factor receptor 1/2

FGR	Fetal growth restriction
GA	Gestational age
GABARAP	GABA type A receptor-associated protein
GEO	Gene expression omnibus
Gly-T	Glycogen-trophoblast
GSK3	Glycogen synthase kinase 3
HDAC6	Histone deacetylase 6
HSP22	Heat shock protein 22
HSP27	Heat shock protein 27
ICM	Inner cell mass
IGF1R	Insulin-like growth factor 1 receptor
IR	Insulin receptor
JNK	c-Jun N-terminal kinase
JZ	Junctional zone
KI	Kinase-inactive
LAB	Labyrinth
LaTP	Labyrinth trophoblast progenitor
MAP2K3/6	Mitogen-activated protein kinase kinase 3/6
MAP2K4/7	Mitogen-activated protein kinase kinase 4/7
MAP3K4	Mitogen-activated protein kinase kinase kinase 4
MAPK	Mitogen-activated protein kinase
MEF-CM	Mouse embryonic fibroblast-conditioned media
NA	Not applicable
NF-kB	Nuclear factor-kappa B
n.s.	Not significant
p-TGC	Parietal-trophoblast giant cell
1° P-TGC	Primary parietal-trophoblast giant cell
2° P-TGC	Secondary parietal-trophoblast giant cell
2° P-TGC P	Secondary parietal-trophoblast giant cell precursor
pAkt	Phosphorylated Akt at Serine 473
pERK	Phosphorylated ERK
pHSP27	Phosphorylated HSP27
pJNK	Phosphorylated JNK
pp38	Phosphorylated p38
qPCR	Quantitative PCR
ROI	Regions of interest
RIPA	Radioimmunoprecipitation assay
RNA-seq	RNA sequencing
RPKM	Reads per kilobase of transcript per million mapped reads
SD	Standard deviation
SDS-PAGE	Sodium dodecyl sulfate polyacrylamide gel electrophoresis
SMF	Stemness maintenance factors
SpA-TGC	Spiral artery-trophoblast giant cell
SpT	Spongiotrophoblast
S-TGC	Sinusoidal-trophoblast giant cell
S-TGC P	Sinusoidal-trophoblast giant cell precursor
SynT	Syncytiotrophoblast
SynTI P	Syncytiotrophoblast I precursor
SynTII P	Syncytiotrophoblast II precursor
TE	Trophectoderm
TS	Trophoblast stem
UV	Ultraviolet
WT	Wild-type

References

1. Woods, L.; Perez-Garcia, V.; Hemberger, M. Regulation of Placental Development and Its Impact on Fetal Growth-New Insights From Mouse Models. *Front. Endocrinol.* **2018**, *9*, 570. [CrossRef]
2. Hemberger, M.; Hanna, C.W.; Dean, W. Mechanisms of early placental development in mouse and humans. *Nat. Rev. Genet.* **2020**, *21*, 27–43. [CrossRef]
3. Brett, K.E.; Ferraro, Z.M.; Yockell-Lelievre, J.; Gruslin, A.; Adamo, K.B. Maternal-fetal nutrient transport in pregnancy pathologies: The role of the placenta. *Int. J. Mol. Sci.* **2014**, *15*, 16153–16185. [CrossRef] [PubMed]
4. Burton, G.J.; Jauniaux, E. Pathophysiology of placental-derived fetal growth restriction. *Am. J. Obstet. Gynecol.* **2018**, *218*, S745–S761. [CrossRef] [PubMed]
5. Tanaka, S.; Kunath, T.; Hadjantonakis, A.K.; Nagy, A.; Rossant, J. Promotion of trophoblast stem cell proliferation by FGF4. *Science* **1998**, *282*, 2072–2075. [CrossRef]
6. Abell, A.N.; Granger, D.A.; Johnson, N.L.; Vincent-Jordan, N.; Dibble, C.F.; Johnson, G.L. Trophoblast stem cell maintenance by fibroblast growth factor 4 requires MEKK4 activation of Jun N-terminal kinase. *Mol. Cell Biol.* **2009**, *29*, 2748–2761. [CrossRef]
7. Zhu, D.; Gong, X.; Miao, L.; Fang, J.; Zhang, J. Efficient Induction of Syncytiotrophoblast Layer II Cells from Trophoblast Stem Cells by Canonical Wnt Signaling Activation. *Stem Cell Rep.* **2017**, *9*, 2034–2049. [CrossRef]
8. Perry, C.H.; Mullins, N.A.; Sweileh, R.B.A.; Shendy, N.A.M.; Roberto, P.A.; Broadhurst, A.L.; Nelson, H.A.; Miranda-Carboni, G.A.; Abell, A.N. MAP3K4 promotes fetal and placental growth by controlling the receptor tyrosine kinases IGF1R/IR and Akt signaling pathway. *J. Biol. Chem.* **2022**, *298*, 102310. [CrossRef] [PubMed]
9. Abell, A.N.; Rivera-Perez, J.A.; Cuevas, B.D.; Uhlik, M.T.; Sather, S.; Johnson, N.L.; Minton, S.K.; Lauder, J.M.; Winter-Vann, A.M.; Nakamura, K.; et al. Ablation of MEKK4 kinase activity causes neurulation and skeletal patterning defects in the mouse embryo. *Mol. Cell Biol.* **2005**, *25*, 8948–8959. [CrossRef]
10. Abell, A.N.; Jordan, N.V.; Huang, W.; Prat, A.; Midland, A.A.; Johnson, N.L.; Granger, D.A.; Mieczkowski, P.A.; Perou, C.M.; Gomez, S.M.; et al. MAP3K4/CBP-regulated H2B acetylation controls epithelial-mesenchymal transition in trophoblast stem cells. *Cell Stem Cell* **2011**, *8*, 525–537. [CrossRef]
11. Mobley, R.J.; Raghu, D.; Duke, L.D.; Abell-Hart, K.; Zawistowski, J.S.; Lutz, K.; Gomez, S.M.; Roy, S.; Homayouni, R.; Johnson, G.L.; et al. MAP3K4 Controls the Chromatin Modifier HDAC6 during Trophoblast Stem Cell Epithelial-to-Mesenchymal Transition. *Cell Rep.* **2017**, *18*, 2387–2400. [CrossRef]
12. Raghu, D.; Mobley, R.J.; Shendy, N.A.M.; Perry, C.H.; Abell, A.N. GALNT3 Maintains the Epithelial State in Trophoblast Stem Cells. *Cell Rep.* **2019**, *26*, 3684–3697 e3687. [CrossRef]
13. He, S.; Nakada, D.; Morrison, S.J. Mechanisms of stem cell self-renewal. *Annu. Rev. Cell Dev. Biol.* **2009**, *25*, 377–406. [CrossRef]
14. Abell, A.N.; Johnson, G.L. MEKK4 is an effector of the embryonic TRAF4 for JNK activation. *J. Biol. Chem.* **2005**, *280*, 35793–35796. [CrossRef]
15. Cuevas, B.D.; Abell, A.N.; Johnson, G.L. Role of mitogen-activated protein kinase kinase kinases in signal integration. *Oncogene* **2007**, *26*, 3159–3171. [CrossRef] [PubMed]
16. Shendy, N.A.M.; Broadhurst, A.L.; Shoemaker, K.; Read, R.; Abell, A.N. MAP3K4 kinase activity dependent control of mouse gonadal sex determination. *Biol. Reprod.* **2021**, *105*, 491–502. [CrossRef] [PubMed]
17. Mobley, R.J.; Abell, A.N. Controlling Epithelial to Mesenchymal Transition through Acetylation of Histone H2BK5. *J. Nat. Sci.* **2017**, *3*, e432.
18. Shendy, N.A.M.; Raghu, D.; Roy, S.; Perry, C.H.; Safi, A.; Branco, M.R.; Homayouni, R.; Abell, A.N. Coordinated regulation of Rel expression by MAP3K4, CBP, and HDAC6 controls phenotypic switching. *Commun. Biol.* **2020**, *3*, 475. [CrossRef] [PubMed]
19. Nelson, H.A.; Mullins, N.A.; Abell, A.N. MAP3K4 signaling regulates HDAC6 and TRAF4 coexpression and stabilization in trophoblast stem cells. *J. Biol. Chem.* **2025**, *301*, 108116. [CrossRef]
20. Jordan, N.V.; Johnson, G.L.; Abell, A.N. Tracking the intermediate stages of epithelial-mesenchymal transition in epithelial stem cells and cancer. *Cell Cycle* **2011**, *10*, 2865–2873. [CrossRef]
21. Nieto, M.A.; Huang, R.Y.; Jackson, R.A.; Thiery, J.P. Emt: 2016. *Cell* **2016**, *166*, 21–45. [CrossRef]
22. Liu, J.; Xu, W.; Sun, T.; Wang, F.; Puscheck, E.; Brigstock, D.; Wang, Q.T.; Davis, R.; Rappolee, D.A. Hyperosmolar stress induces global mRNA responses in placental trophoblast stem cells that emulate early post-implantation differentiation. *Placenta* **2009**, *30*, 66–73. [CrossRef]
23. Yang, Y.; Arenas-Hernandez, M.; Gomez-Lopez, N.; Dai, J.; Parker, G.C.; Puscheck, E.E.; Rappolee, D.A. Hypoxic Stress Forces Irreversible Differentiation of a Majority of Mouse Trophoblast Stem Cells Despite FGF4. *Biol. Reprod.* **2016**, *95*, 110. [CrossRef]
24. Oke, S.L.; Hardy, D.B. The Role of Cellular Stress in Intrauterine Growth Restriction and Postnatal Dysmetabolism. *Int. J. Mol. Sci.* **2021**, *22*, 6986. [CrossRef]
25. Vidyasagar, A.; Wilson, N.A.; Djamali, A. Heat shock protein 27 (HSP27): Biomarker of disease and therapeutic target. *Fibrogenes. Tissue Repair.* **2012**, *5*, 7. [CrossRef]

26. Tedesco, B.; Cristofani, R.; Ferrari, V.; Cozzi, M.; Rusmini, P.; Casarotto, E.; Chierichetti, M.; Mina, F.; Galbiati, M.; Piccolella, M.; et al. Insights on Human Small Heat Shock Proteins and Their Alterations in Diseases. *Front. Mol. Biosci.* **2022**, *9*, 842149. [CrossRef]
27. Haidar, M.; Asselbergh, B.; Adriaenssens, E.; De Winter, V.; Timmermans, J.P.; Auer-Grumbach, M.; Juneja, M.; Timmerman, V. Neuropathy-causing mutations in HSPB1 impair autophagy by disturbing the formation of SQSTM1/p62 bodies. *Autophagy* **2019**, *15*, 1051–1068. [CrossRef]
28. Katsogiannou, M.; Andrieu, C.; Rocchi, P. Heat shock protein 27 phosphorylation state is associated with cancer progression. *Front. Genet.* **2014**, *5*, 346. Erratum in *Front Genet.* **2025**, *16*, 1703072. [CrossRef] [PubMed]
29. Sluzala, Z.B.; Hamati, A.; Fort, P.E. Key Role of Phosphorylation in Small Heat Shock Protein Regulation via Oligomeric Disaggregation and Functional Activation. *Cells* **2025**, *14*, 127. [CrossRef] [PubMed]
30. Zeke, A.; Misheva, M.; Remenyi, A.; Bogoyevitch, M.A. JNK Signaling: Regulation and Functions Based on Complex Protein-Protein Partnerships. *Microbiol. Mol. Biol. Rev.* **2016**, *80*, 793–835. [CrossRef] [PubMed]
31. Shendy, N.A.M.; Abell, A.N. MAP Kinase Cascades. In *Encyclopedia of Molecular Pharmacology*; Springer: Berlin/Heidelberg, Germany, 2021.
32. Rappolee, D.A.; Awonuga, A.O.; Puscheck, E.E.; Zhou, S.; Xie, Y. Benzopyrene and experimental stressors cause compensatory differentiation in placental trophoblast stem cells. *Syst. Biol. Reprod. Med.* **2010**, *56*, 168–183. [CrossRef]
33. Marsh, B.; Blelloch, R. Single nuclei RNA-seq of mouse placental labyrinth development. *Elife* **2020**, *9*, e60266. [CrossRef] [PubMed]
34. Jiang, X.; Wang, Y.; Xiao, Z.; Yan, L.; Guo, S.; Wang, Y.; Wu, H.; Zhao, X.; Lu, X.; Wang, H. A differentiation roadmap of murine placentation at single-cell resolution. *Cell Discov.* **2023**, *9*, 30. [CrossRef]
35. Alvarez-Sanchez, A.; Grinat, J.; Doria-Borrell, P.; Mellado-Lopez, M.; Pedrera-Alcocer, E.; Malenchini, M.; Meseguer, S.; Hemberger, M.; Perez-Garcia, V. The GPI-anchor biosynthesis pathway is critical for syncytiotrophoblast differentiation and placental development. *Cell Mol. Life Sci.* **2024**, *81*, 246. [CrossRef] [PubMed]
36. Ueno, M.; Lee, L.K.; Chhabra, A.; Kim, Y.J.; Sasidharan, R.; Van Handel, B.; Wang, Y.; Kamata, M.; Kamran, P.; Sereti, K.I.; et al. c-Met-dependent multipotent labyrinth trophoblast progenitors establish placental exchange interface. *Dev. Cell* **2013**, *27*, 373–386. [CrossRef]
37. Cristofani, R.; Piccolella, M.; Crippa, V.; Tedesco, B.; Montagnani Marelli, M.; Poletti, A.; Moretti, R.M. The Role of HSPB8, a Component of the Chaperone-Assisted Selective Autophagy Machinery, in Cancer. *Cells* **2021**, *10*, 335. [CrossRef]
38. Nivon, M.; Abou-Samra, M.; Richet, E.; Guyot, B.; Arrigo, A.P.; Kretz-Remy, C. NF-kappaB regulates protein quality control after heat stress through modulation of the BAG3-HspB8 complex. *J. Cell Sci.* **2012**, *125*, 1141–1151. [CrossRef]
39. Nivon, M.; Fort, L.; Muller, P.; Richet, E.; Simon, S.; Guey, B.; Fournier, M.; Arrigo, A.P.; Hetz, C.; Atkin, J.D.; et al. NFkappaB is a central regulator of protein quality control in response to protein aggregation stresses via autophagy modulation. *Mol. Biol. Cell* **2016**, *27*, 1712–1727. [CrossRef]
40. Bonavita, R.; Vitale, F.; Verdicchio, L.V.; Williams, S.V.; Caporaso, M.G.; Fleming, A.; Renna, M. Small HSPs at the crossroad between protein aggregation, autophagy and unconventional secretion: Clinical implications and potential therapeutic opportunities in the context of neurodegenerative diseases. *Front. Cell Dev. Biol.* **2025**, *13*, 1538377. [CrossRef]
41. Rusmini, P.; Cristofani, R.; Galbiati, M.; Cicardi, M.E.; Meroni, M.; Ferrari, V.; Vezzoli, G.; Tedesco, B.; Messi, E.; Piccolella, M.; et al. The Role of the Heat Shock Protein B8 (HSPB8) in Motoneuron Diseases. *Front. Mol. Neurosci.* **2017**, *10*, 176. [CrossRef] [PubMed]
42. Chierichetti, M.; Cristofani, R.; Crippa, V.; Ferrari, V.; Cozzi, M.; Casarotto, E.; Pramaggiore, P.; Cornaggia, L.; Patelli, G.; Mohamed, A.; et al. Small heat shock protein B8: From cell functions to its involvement in diseases and potential therapeutic applications. *Neural Regen. Res.* **2025**, *20*, 2872–2886. [CrossRef] [PubMed]
43. Singh, A.; Perez, M.L.; Kirsanov, O.; Padilla-Banks, E.; Guardia, C.M. Autophagy in reproduction and pregnancy-associated diseases. *iScience* **2024**, *27*, 111268. [CrossRef] [PubMed]
44. Zhou, P.; Wang, J.; Wang, J.; Liu, X. When autophagy meets placenta development and pregnancy complications. *Front. Cell Dev. Biol.* **2024**, *12*, 1327167. [CrossRef]
45. Carvajal, L.; Gutierrez, J.; Morselli, E.; Leiva, A. Autophagy Process in Trophoblast Cells Invasion and Differentiation: Similitude and Differences With Cancer Cells. *Front. Oncol.* **2021**, *11*, 637594. [CrossRef]
46. Aoki, A.; Nakashima, A.; Kusabiraki, T.; Ono, Y.; Yoshino, O.; Muto, M.; Kumasawa, K.; Yoshimori, T.; Ikawa, M.; Saito, S. Trophoblast-Specific Conditional Atg7 Knockout Mice Develop Gestational Hypertension. *Am. J. Pathol.* **2018**, *188*, 2474–2486. [CrossRef]
47. Muralimanoharan, S.; Gao, X.; Weintraub, S.; Myatt, L.; Maloyan, A. Sexual dimorphism in activation of placental autophagy in obese women with evidence for fetal programming from a placenta-specific mouse model. *Autophagy* **2016**, *12*, 752–769. [CrossRef] [PubMed]
48. Hung, T.H.; Hsieh, T.T.; Chen, S.F.; Li, M.J.; Yeh, Y.L. Autophagy in the human placenta throughout gestation. *PLoS ONE* **2013**, *8*, e83475. [CrossRef] [PubMed]

49. Oh, S.Y.; Roh, C.R. Autophagy in the placenta. *Obstet. Gynecol. Sci.* **2017**, *60*, 241–259. [CrossRef]
50. Chakraborty, S.; Bose, R.; Islam, S.; Das, S.; Ain, R. Harnessing Autophagic Network Is Essential for Trophoblast Stem Cell Differentiation. *Stem Cells Dev.* **2020**, *29*, 682–694. [CrossRef]
51. Levine, B.; Kroemer, G. Biological Functions of Autophagy Genes: A Disease Perspective. *Cell* **2019**, *176*, 11–42. [CrossRef]
52. Kostenko, S.; Moens, U. Heat shock protein 27 phosphorylation: Kinases, phosphatases, functions and pathology. *Cell Mol. Life Sci.* **2009**, *66*, 3289–3307. [CrossRef]
53. Heberle, A.M.; Razquin Navas, P.; Langelaar-Makkinje, M.; Kasack, K.; Sadik, A.; Faessler, E.; Hahn, U.; Marx-Stoelting, P.; Opitz, C.A.; Sers, C.; et al. The PI3K and MAPK/p38 pathways control stress granule assembly in a hierarchical manner. *Life Sci. Alliance* **2019**, *2*, e201800257. [CrossRef]
54. Jee, B.; Dhar, R.; Singh, S.; Karmakar, S. Heat Shock Proteins and Their Role in Pregnancy: Redefining the Function of "Old Rum in a New Bottle". *Front. Cell Dev. Biol.* **2021**, *9*, 648463. [CrossRef]
55. Ruane, P.T.; Koeck, R.; Berneau, S.C.; Kimber, S.J.; Westwood, M.; Brison, D.R.; Aplin, J.D. Osmotic stress induces JNK-dependent embryo invasion in a model of implantation. *Reproduction* **2018**, *156*, 421–428. [CrossRef]
56. Adams, R.H.; Porras, A.; Alonso, G.; Jones, M.; Vintersten, K.; Panelli, S.; Valladares, A.; Perez, L.; Klein, R.; Nebreda, A.R. Essential role of p38alpha MAP kinase in placental but not embryonic cardiovascular development. *Mol. Cell* **2000**, *6*, 109–116. [CrossRef]
57. Mauthe, M.; Orhon, I.; Rocchi, C.; Zhou, X.; Luhr, M.; Hijlkema, K.J.; Coppes, R.P.; Engedal, N.; Mari, M.; Reggiori, F. Chloroquine inhibits autophagic flux by decreasing autophagosome-lysosome fusion. *Autophagy* **2018**, *14*, 1435–1455. [CrossRef]
58. Love, M.I.; Huber, W.; Anders, S. Moderated estimation of fold change and dispersion for RNA-seq data with DESeq2. *Genome Biol.* **2014**, *15*, 550. [CrossRef]
59. Wickham, H.; Averick, M.; Bryan, J.; Chang, W.; D'Agostino McGowan, L.; Francois, R.; Grolemund, G.; Hayes, A.; Henry, L.; Hester, J.; et al. Welcome to the tidyverse. *J. Open Source Softw.* **2019**, *4*, 1686. [CrossRef]

Disclaimer/Publisher's Note: The statements, opinions and data contained in all publications are solely those of the individual author(s) and contributor(s) and not of MDPI and/or the editor(s). MDPI and/or the editor(s) disclaim responsibility for any injury to people or property resulting from any ideas, methods, instructions or products referred to in the content.